

Attenuation of sunlight measured from moored radiometers to assess depletion of suspended particles caused by bivalve aquaculture

Diego A. Ibarra^{1*}, Allan Cembella², and Jon Grant¹

¹Department of Oceanography, Dalhousie University, 1355 Oxford Street, PO BOX 15000, Halifax, Nova Scotia, B3H 4R2, Canada

²Alfred Wegener Institute for Polar and Marine Research, Am Handelshafen 12, D-27570, Bremerhaven, Germany

Abstract

Bivalve suspension-feeding can produce horizontal gradients of particulate suspended matter, or seston, which may impair bivalve growth among other impacts to the coastal ecosystem. We proposed a method to assess the concentration of seston at different locations along a shellfish farm by means of measurements of the depth-averaged diffuse attenuation coefficient of downwelling irradiance at 490 nm, \bar{K} , from at least two autonomous buoys equipped with a vertical array of irradiance sensors. Two approaches were compared. First, horizontal gradients of chlorophyll plus phaeopigments (Chl) were calculated from \bar{K} using an empirical algorithm derived from water samples. In the second approach, gradients of particulate suspended matter were calculated after correcting \bar{K} for the attenuation due to water and riverine colored dissolved organic matter (CDOM), estimated from continuous in situ measurements of salinity. The method was assessed in a mussel farm in Ship Harbour (Nova Scotia, Canada). The proposed method is relatively insensitive to the angular distribution of downwelling irradiance, biofouling, frame-shading, and wave focusing; but it cannot be easily applied in places with strong and sustained sediment resuspension. This method can complement and validate current modeling studies of seston depletion, and it can assist managerial activities and legislative requirements of shellfish aquaculture. This method can also be used to assess gradients of other ecologically relevant substances (i.e., CDOM, phytoplankton, and seston) in applications associated with sewage discharges, river runoff, harmful algal blooms, suspension-feeding invasive bivalves, and other horizontally variable phenomena in the coastal ocean.

Cultured bivalves can produce, via filter-feeding, spatial gradients of suspended particles or seston (Pilditch et al. 2001; Grant et al. 2008). The term “seston depletion” (Wildish and Kristmanson 1997) refers to the process by which these gradients of seston concentration are formed when the supply of seston by currents and turbulent mixing cannot offset the demand by bivalve feeding (Pilditch et al. 2001). Seston deple-

tion has the potential to impair bivalve growth (Fréchette and Bourget 1985; Strohmeier et al. 2008) and to alter the ecosystem (Smaal et al. 2001). The economical and ecological consequences associated with seston depletion have instigated research to measure and predict spatial gradients of seston concentration (e.g., Incze et al. 1981; Guyondet et al. 2010).

In principle, measuring horizontal gradients of seston requires simultaneous measurements, at different locations along a farm (minimum of two), of the concentration of a tracer that is (1) naturally occurring, (2) conservative, and (3) filtered with high efficiency by the bivalves. Although the tracer needs to be a proxy for the nutritional value of seston to predict bivalve growth, which is a primary goal in carrying capacity studies (e.g., Grant and Bacher 1998; Pouvreau et al. 2000; Ferreira et al. 2008), nutritional information is irrelevant for the assessment of spatial gradients of seston, which is the focus of this study. Chlorophyll *a* (Chl *a*) has been considered the natural tracer in most previous studies (e.g., Fréchette et al. 1991; Heasman et al. 1998), however other tracers also have been used (total particulate matter: Prins et al. 1996; particulate carbon: Cabanas et al. 1979; particulate silicate: Dame et al. 1991, etc.).

*Corresponding author: E-mail: Diego.Ibarra@dal.ca

Acknowledgments

We thank J. Stairs and AquaPrime Mussel Ranch, Ltd. for their invaluable help in the logistics of this research; T. Windust, S. Kirchhoff, C. Rafuse, S. Pereira, A. Martínez and N. Lewis for their collaboration in the field; J. J. Cullen, P. Cranford, M. Lewis, Y. Huot, and two anonymous reviewers for the insightful comments and R. Boyce and the Bedford Institute of Oceanography for processing the salinity samples. This research was funded by the National Research Council/NSERC Research Partnership (A.C.), AquaNET – Canada’s Network of Centres of Excellence in Aquaculture (A.C.), and the International Council for Canadian Studies (D.I.).

DOI 10.4319/lom.2012.10.1051

Regardless the tracer, it is difficult to demonstrate statistically significant differences in the time-averaged concentration of tracer among tested locations, because all these tracers are subject to vertical, horizontal, and temporal sources of variation that can overwhelm the effect of bivalve filter-feeding. The effect of high tracer variability is particularly problematic in experiments conducted in farms where bivalves are reared spread out over vast areas, and when using sampling approaches that are limited in their vertical resolution (e.g., moored fluorometer and transmissometer: Pilditch et al. 2001), their temporal resolution (e.g., monthly fluorometer vertical casts: Ogilvie et al. 2000), or both (water samples: Rosenberg and Loo 1983; fluorometer horizontal transects: Fr chet te et al. 1991; Grant et al. 2008).

We propose a method to assess horizontal gradients of seston concentration using semicontinuous measurements that are water column-integrated. The method uses autonomous buoys deployed at different locations along a farm. The buoys are equipped with a vertical array of irradiance sensors to estimate the depth-averaged diffuse attenuation coefficient of downwelling irradiance at 490 nm, as a proxy for tracer concentration. Note that, using irradiance sensors that integrate over the photosynthetic available radiation spectrum (i.e., PAR), produce diffuse attenuation coefficients for PAR (i.e., K_{PAR}), which vary as a function of depth (Lee et al. 2007). Therefore, monochromatic radiometers are preferred.

In general terms, the diffuse attenuation coefficient of downwelling irradiance (K ; m^{-1} ; see Table 1 for more symbols and units) represents the rate of decrease of downwelling irradiance (E ; $\mu\text{W cm}^{-2} \text{nm}^{-1}$) with increasing depth (z ; m), as defined by Eq. 1 (Kirk 1994). For simplicity, wavelength dependencies are ignored and the sub-index ‘‘d,’’ commonly used to represent downwelling radiant flux (e.g., K_d and E_d), is omitted.

$$K = -\frac{1}{E} \frac{dE}{dz} \quad (1)$$

The attenuation coefficient, K , depends on the inherent optical properties of the medium (i.e., IOPs) and the distribution of the light field, as expressed by the following approximation (Sathyendranath and Platt 1988):

$$K = \frac{a + b_b}{\bar{\mu}} \quad (2)$$

The absorption and backscattering coefficients (a and b_b ; m^{-1}) define the IOPs and the average cosine for downwelling irradiance ($\bar{\mu}$; dimensionless; sub-index ‘‘d’’ is also omitted) defines the distribution of the light field.

Because of the additive nature of the IOPs, K can be partitioned into partial attenuation coefficients, each corresponding to a different component of the medium (Kirk 1994): pure ocean water (K_w), colored dissolved organic matter (CDOM) or gelbstoff (K_g), and seston or particles (K_p), which can be further divided into phytoplankton (K_ϕ) and non-algal particles (i.e., tripton; K_t):

$$K = K_\phi + K_t + K_g + K_w \quad (3)$$

In the context of assessing spatial gradients of tracer concentration, the goal is to discriminate the portion of K attributable to the filterable tracer from and the portion of K due to nonfilterable substances. In the simplest scenario, the values of K_g , K_t , and K_w are either negligible or constant throughout the experiment and the only source of variation of K is the concentration of phytoplankton, which is considered the filterable tracer. In this case, the offset due to non-tracer attenuation is considered constant over time and is determined empirically through a regression between Chl a plus phaeopigments (i.e., Chl) and the attenuation coefficient K (i.e., approach based on Chl: K regression). In a complex scenario, where K_w is constant but K_g , K_t , and K_ϕ are not negligible and vary over time, an independent dataset will be required to distinguish between tracer and nonfilterable components of K . (i.e., approach based on CDOM-correction) Both, Chl: K regression and CDOM-correction approaches are described, assessed, and compared in the present study. The new ecological insights that have resulted from the application of this method are shown elsewhere (Ibarra 2003).

Materials and procedures

General approach

The fraction of tracer remaining at location x (m) inside a bivalve farm with respect to a reference upstream location (i.e., seston depletion index or D ; dimensionless), is estimated using simultaneous measurements of K at the inside and reference locations. The measurements of K can be used to estimate the depletion index using two different approaches: (1) Chl: K regression and (2) CDOM correction. To differentiate the results from these two approaches, output from the Chl: K regression approach will be referred to as the Chl-based depletion index (D_{chl}) and output from the CDOM-correction approach will be referred to as particle-based depletion index (D_p). The data collected and the post-collection data processing were different for these approaches; therefore details will be explained in separate sections.

Study site

All assessment experiments were conducted in a mussel farm (660 \times 330 m) in Ship Harbour, Nova Scotia, Canada (Fig. 1). This estuarine fjord has semidiurnal tides (average range: 1.4 m) and receives the discharge of CDOM-rich freshwater from the Ship Harbour River at an annual average flow rate of 18 $\text{m}^3 \text{s}^{-1}$ (Gregory et al. 1993). Cultured mussels (*Mytilus edulis* and *M. trossolus*) are reared on long-lines, which are 120 m ropes kept at approximately 4 m below surface using buoys and concrete blocks. Cultured mussels are attached to 4 m ropes that hung vertically from the long-lines, therefore the bivalve stratum was defined by an upper boundary ($z_U = 4$ m) and a lower boundary ($z_L = 8$ m; Fig. 2).

Table 1. Symbols used in this study.

Symbol	Units	Definition
$\bar{\mu}$	dimensionless	Average cosine for downwelling irradiance
β	dimensionless	Fraction of irradiance reduced by biofouling, frame-shading, and/or calibration errors
a	m^{-1}	Absorption coefficient
a_g	m^{-1}	Absorption coefficient for gelbstoff or CDOM
a_p	m^{-1}	Absorption coefficient for particles
a_w	m^{-1}	Absorption coefficient for water
a_ϕ^*	$m^2 \text{ mg Chl}^{-1}$	Specific absorption coefficient of phytoplankton
b	m^{-1}	Scattering coefficient
b_p	m^{-1}	Scattering coefficient for particles
b_b	m^{-1}	Backscattering coefficient
$b_{b,p}$	m^{-1}	Backscattering coefficient for particles
$b_{b,\phi}^*$	$m^2 \text{ mg Chl}^{-1}$	Specific backscattering coefficient of phytoplankton
Chl	mg m^{-3}	Concentration of Chl <i>a</i> plus phaeopigments
D_{Chl}	dimensionless	Chl-based depletion index measured using the constant offset approach
D_p	dimensionless	Particle-based depletion index measured using the time-varying offset approach
E	$\mu\text{W cm}^{-2} \text{ nm}^{-1}$	Downwelling irradiance
K	m^{-1}	Diffuse attenuation coefficient of downwelling irradiance
K_ϕ	m^{-1}	Partial attenuation coefficient for phytoplankton
K_t	m^{-1}	Partial attenuation coefficient for tripton
K_p	m^{-1}	Partial attenuation coefficient for particles
K_g	m^{-1}	Partial attenuation coefficient for gelbstoff
K_w	m^{-1}	Partial attenuation coefficient for water
\bar{K}	m^{-1}	Depth-averaged ($z_4 \rightarrow z_8$) diffuse attenuation coefficient of downwelling irradiance at 490 nm
m_{Chl}	$m^2 \text{ mg}^{-1}$	Slope of the regression between Chl and \bar{K}
m_g	m^{-1}	Slope of the regression between salinity and a_g
n	counts	Sample number
N	counts	Number of particles in a solution of volume V
n_{Chl}	m^{-1}	Intercept of the regression between Chl and \bar{K}
n_g	m^{-1}	Intercept of the regression between salinity and a_g
Q_a	m part^{-1}	Absorption efficiency factor
Q_{hb}	m part^{-1}	Backscattering efficiency factor
r_p	m	Equivalent radius of a phytoplankter
r	m	Equivalent radius of a faecal-pellet
\bar{S}	dimensionless	In situ salinity at 4.5 m from sea bottom
s	m^2	Cross-sectional area of a particle
t	s	Local time, GMT – 3
V	m^3	Volume of a solution with N seston particles
x	m	Distance along the main current axis of the farm
z	m	Depth
z_U	m	Upper boundary of the mussel layer (i.e., 4 m)
z_L	m	Lower boundary of the mussel layer (i.e., 8 m)

Water sampling

Mussel filtration was expected to cause persistent gradients of phytoplankton, with the minimum concentration located at the mid-stratum depth [i.e., $(z_L + z_U)/2$]. Therefore, for the development of calibration and correction algorithms, we needed to collect water samples representative of the entire bivalve stratum. There are techniques to obtain water-column integrated samples (e.g., Sutherland et al. 1992; Huang et al. 2003). However, here we collected multiple samples at three

discrete depths: 20% of the samples were collected at z_U , 20% at z_L , and 60% at the mid-stratum depth. Sample average is analog to a weighed average, where most of the weight lays at mid-stratum depth. Water samples were collected weekly. On each sampling day, the boat was anchored approximately 10 m away from the optical instruments (to avoid sensor shading, see section below). A 5-L Niskin bottle was used to collect five samples: One sample at z_U (i.e., 4 m), one at z_L (i.e., 8 m), and three at mid-stratum depth (i.e., 6 m); each sample (8 L)

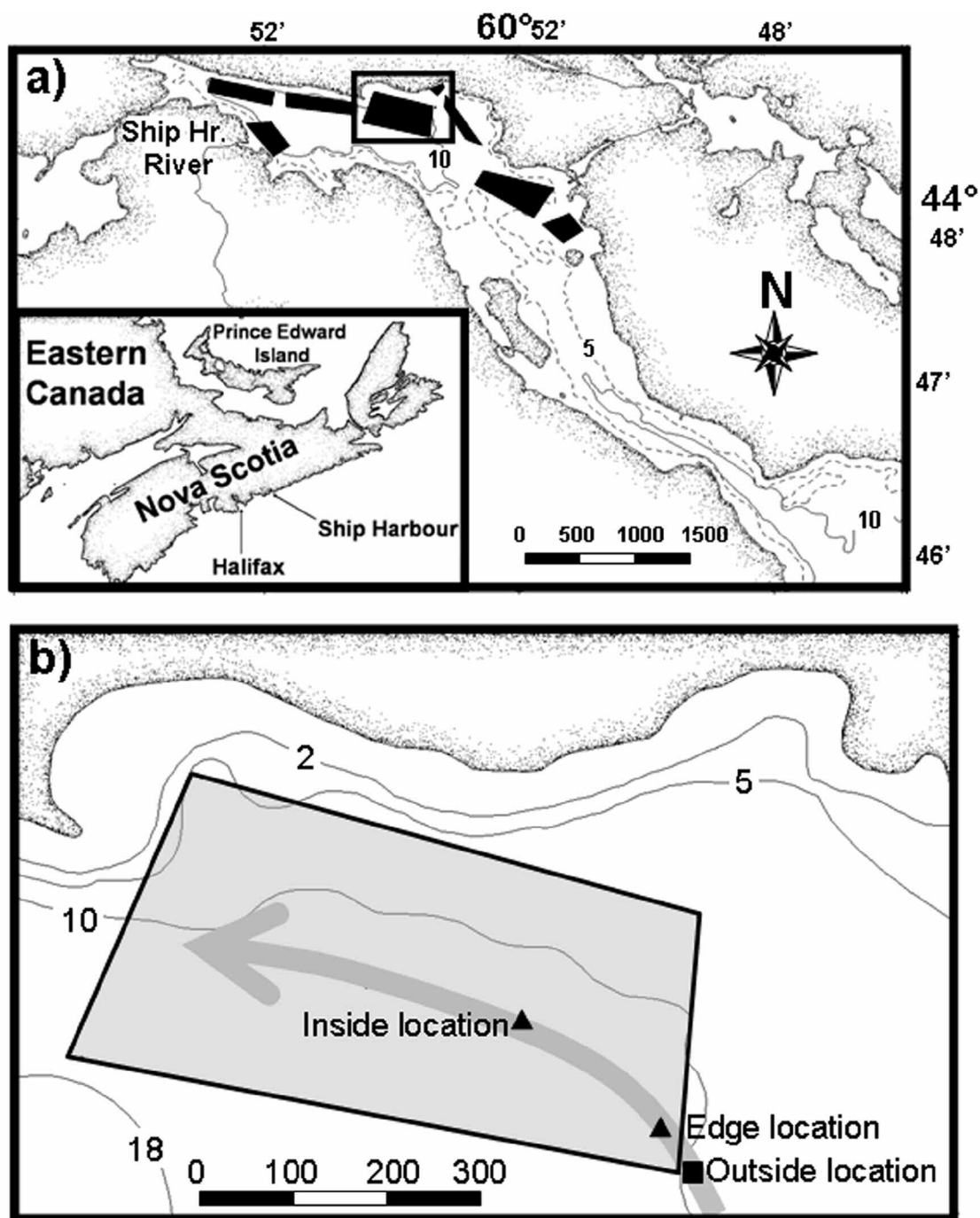


Fig. 1. a) Ship Harbour, Nova Scotia, Canada ($44^{\circ}48'36.18''\text{N}$, $62^{\circ}50'58.32''\text{W}$). Mussel leases are shown as black polygons. The square encompasses the study lease, which is shown in detail in panel b. b) The gray polygon represents the area occupied by mussel long-lines. The two tested locations (triangles) were compared against the reference (square). The arrow represents the direction of the dominant currents. Depth contours and distances are expressed in meters.

requiring the content of two Niskin bottle casts deployed consecutively. The time required to collect all five samples was approximately 10 minutes. Both stations (inside and outside the farm) were sampled and the elapsed time between sampling the two stations was approximately 1 h. After collection,

samples were immediately placed in dark, thermo-insulated, 8-L containers. From each sample, aliquots were sub-sampled to measure the concentration of Chl *a* and phaeopigments (for the Chl:K regression approach), salinity, and absorption spectra of CDOM (for the CDOM-correction approach) and

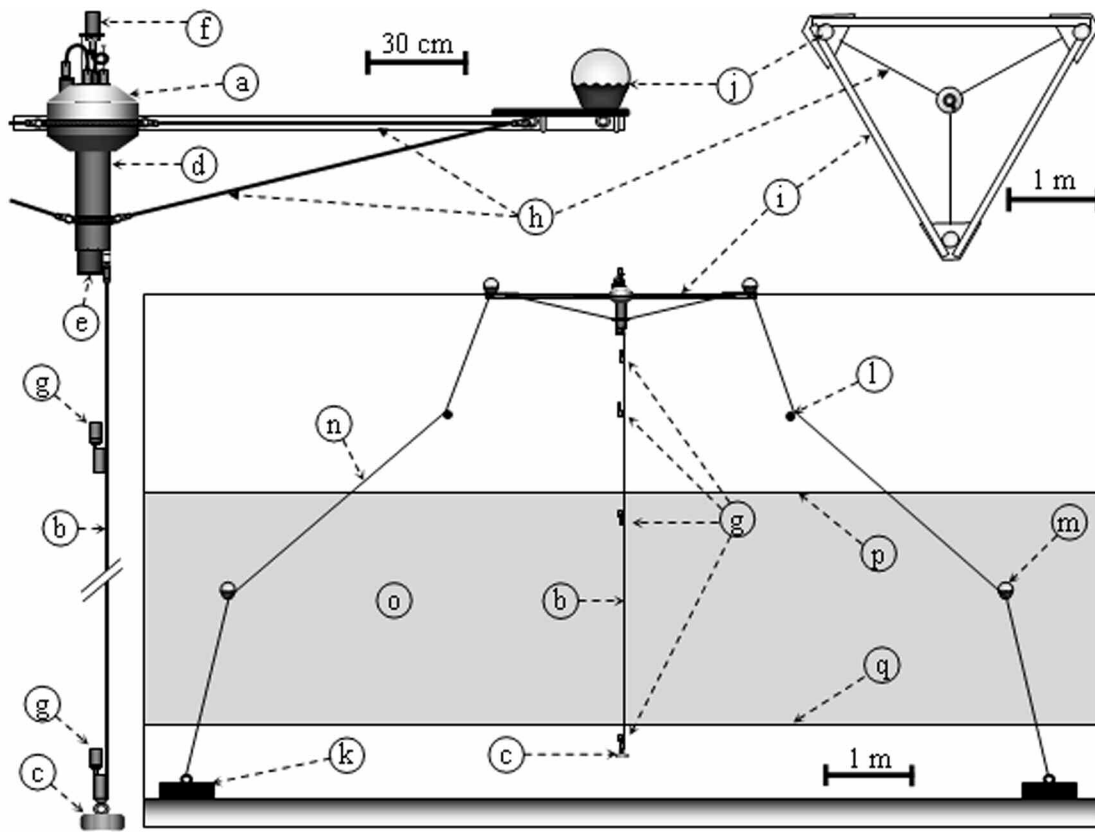


Fig. 2. Schematic of a Tethered Attenuation Coefficient Chain Sensor (TACCS; Satlantic). The instrument consists of a floating buoy (a) with a chain of radiometers (b) that is kept vertical by a 1 kg weight at the end of the chain (c). The data-logger (d) stores data from 7 sensors of upwelling radiance (e) and 5 sensors of downwelling irradiance at 490 nm, one above surface (f) and four on the chain (g). Three elastic tensors (h) hold TACCS in place within a frame made with PVC pipe (i). The frame was kept afloat helped by surface buoys (j), and it was anchored with three 40 kg concrete blocks (k). A combination of weights (l) and floats (m) on the anchoring lines (n) prevented the lines to becoming too slack during low tide. The gray region (o) represents the bivalve stratum and is defined by the upper boundary $z_U = 4$ m (p) and the lower boundary $z_L = 8$ m (q).

organic and inorganic particulate matter (i.e., POM and PIM; for the section of sediment resuspension). All samples were filtered and preserved or extracted within 2 h of collection.

Optical instruments and measurements

The optical instruments used in this study were two Tethered Attenuation Coefficient Chain Sensors (TACCS; Satlantic). These autonomous buoys, originally designed to groundtruth SeaWiFS satellite images, were adapted for long-term deployments using a floating black frame constructed with PVC pipe. Details of TACCS, the frame, and the anchoring system are shown in Fig. 2. The radiometers on the vertical array measured downwelling irradiance at 490 nm (spectral bandwidth = 10 nm), using a 13 mm² silicon photodiode with an 86 mm² cosine collector and a low fluorescence interference filter. Although TACCS measured downwelling irradiance at 4 depths, only measurements at the upper (z_U ; m) and lower (z_L ; m) boundaries of the stratum where bivalves were concentrated were used in this study. The TACCS were programmed to turn on at 0500 hour and sample until 2100 hour. Measurements were taken continuously for 3 s every

minute at sampling rate of 3 Hz. The TACCS were also programmed to turn on at 0200 hour and sample for 5 min to estimate instrument noise and dark currents (i.e., mean irradiance in the absence of signal). Sensor cleaning, data download, and battery replacement (two alkaline 9 V), were conducted weekly.

The diffuse attenuation coefficient of downwelling irradiance at 490 nm, measured at distance x (m) along the farm, at local time t (s; GMT-3) and averaged over the bivalve stratum [i.e., $K(490, z_U \rightarrow z_L, x, t)$; m⁻¹], was calculated from each of the buoys using the integration of Eq. 1 between the upper and lower boundary depths of the bivalve stratum:

$$\bar{K}(x, t) = K(490, z_U \rightarrow z_L, x, t) = \frac{-\ln\left(\frac{E(z_L, x, t)}{E(z_U, x, t)}\right)}{z_L - z_U} \quad (4)$$

For simplicity, an overbar (i.e., \bar{K}) will be used to express diffuse attenuation depth-averaged over the bivalve stratum and at 490 nm. The data points of $E(z_U, x, t)$ and $E(z_L, x, t)$ are the

time-series of downwelling irradiance at upper and lower boundary depths, respectively.

The mean dark current for each E sensor was estimated by averaging all the data points measured at night between 0200 and 0205 h. The mean dark current for each sensor was subtracted from their respective E time-series. Regardless of this dark current correction, the data points of $E(x,t)$ recorded in early morning and late evening were distorted as the magnitude of the signal approached the magnitude of the noise. Therefore, we discarded E data points smaller than 100 times the noise magnitude. The noise for each sensor was defined as the mean difference between the highest and lowest values measured each night, after outliers were removed. We deemed as outliers a few data points where E was greater than $5 \mu\text{W cm}^{-2} \text{ nm}^{-1}$, which likely occurred as a result of lights onboard boats navigating close to our instrument buoys. For this study, the average noise from all the sensors of the two TACCS was $0.021 \pm 0.004 \mu\text{W cm}^{-2} \text{ nm}^{-1}$; thus data below $2 \mu\text{W cm}^{-2} \text{ nm}^{-1}$ was discarded.

Approach based on Chl:K regression

In the simplest scenario, \bar{K}_g , \bar{K}_l , and \bar{K}_w are negligible, constant, or covarying with \bar{K} , and \bar{K}_ϕ is the main source of variability of \bar{K} . Phytoplankton is conceived as the natural filterable tracer and the approach to estimate tracer concentration consists in regressing the instrument measurements (i.e., $\bar{K}(x,t)$) against a proxy for phytoplankton biomass. In this study, we used the concentration of Chl a plus phaeopigments (Chl; mg m^{-3}) as the proxy for phytoplankton biomass.

For the determination of Chl, discrete water samples were collected as previously described and 100 mL triplicate aliquots were filtered onto Whatman GF/F glass fiber filters (nominal pore size $0.7 \mu\text{m}$). Filters were placed in 10 mL pre-chilled 90% acetone and then transported to the laboratory in a dark container with dry ice (-78.5°C). Concentrations of Chl a and phaeopigments were determined fluorometrically according to the method of Strickland and Parsons (1972) after a 24-h extraction period. Reported Chl concentrations are the average of the five samples (i.e., average of fifteen aliquots) collected throughout the bivalve stratum.

The averaged Chl concentrations were regressed against the values of $\bar{K}(x,t)$ measured at the same time as the water samples were collected. The calculated linear regression was used to convert the time-series of $\bar{K}(x,t)$ into a time-series of Chl concentration ($\text{Chl}(x,t)$, mg m^{-3}). The algorithm, expressed in terms of Chl, is described by the following equation:

$$\text{Chl}(x,t) = \frac{\bar{K}(x,t) - n_{\text{Chl}}}{m_{\text{Chl}}} \quad (5)$$

where the coefficient m_{Chl} ($\text{m}^2 \text{ mg}^{-1}$) is the slope of the linear regression between Chlorophyll and $\bar{K}(x,t)$, and n_{Chl} (m^{-1}) is the value of \bar{K} when Chl is zero (i.e., intercept). The value of n_{Chl} is the attenuation offset due to nontracer substances and is considered to remain constant over the experiment.

The ratio between the \bar{K} -estimated pigments inside the farm, $\text{Chl}(x,t)$, and outside the farm, $\text{Chl}(0,t)$, was used to cal-

culate the instantaneous Chl-based depletion index [$D_{\text{Chl}}(x,t)$; dimensionless], which approximates the fraction of pigments remaining after mussel feeding at time t and at location x along the farm:

$$D_{\text{Chl}}(x,t) = \frac{\text{Chl}(x,t)}{\text{Chl}(0,t)} = \frac{\bar{K}(x,t) - n_{\text{Chl}}}{\bar{K}(0,t) - n_{\text{Chl}}} \quad (6)$$

We assumed that the slope m_{Chl} inside the farm is the same as outside the farm. Due to the close proximity of the two stations ($<300 \text{ m}$; see Fig. 1), this assumption seems reasonable for this study. However, in cases where the m_{Chl} slopes inside and outside the farm are different, then Eq. 6 will not hold true. The m_{Chl} and n_{Chl} coefficients used in this study are shown in Fig. 3a.

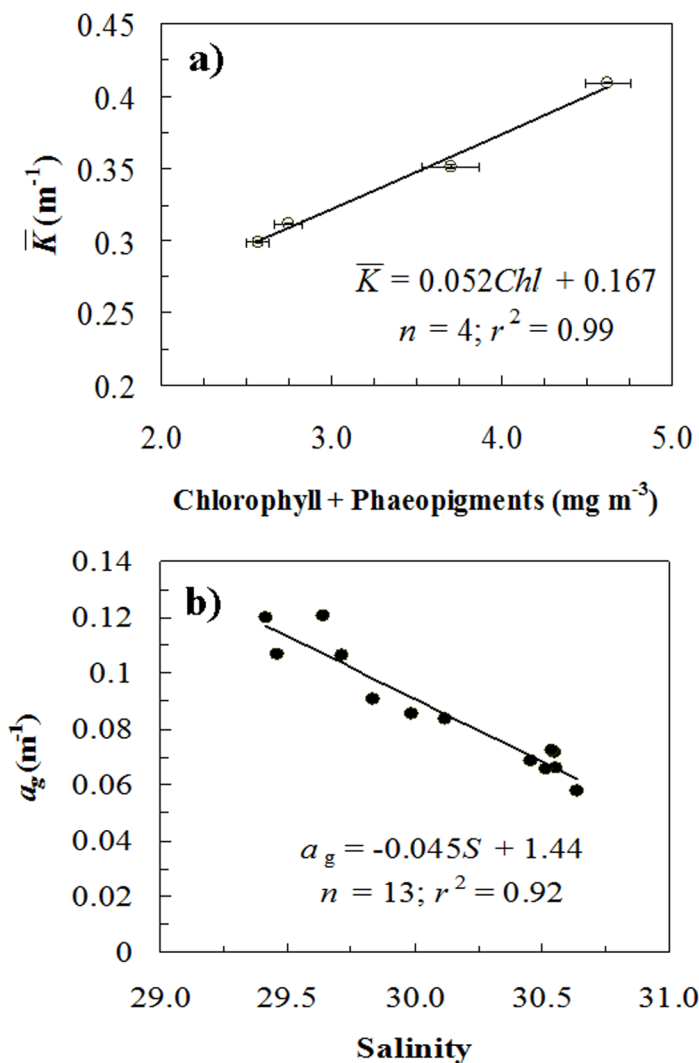


Fig. 3. a) Linear regression between chlorophyll plus phaeopigments (Chl) and the depth-averaged diffuse attenuation coefficient at 490 nm (\bar{K}). Error bars signify 1 standard error. b) Linear regression between salinity (S) and the absorption coefficient of color dissolved organic matter at 490 nm (a_g). Times of sample collection are shown in Fig. 4c and Fig. 5c.

The average Chl-based depletion index ($\bar{D}_{Chl}(x)$; dimensionless) at location x inside the farm was calculated as the average $Chl(x,t)$ divided by the average $Chl(0,t)$:

$$\bar{D}_{Chl}(x) = \frac{\sum Chl(x,t)}{\sum Chl(0,t)} = \frac{\sum [\bar{K}(x,t) - n_{Chl}]}{\sum [\bar{K}(0,t) - n_{Chl}]} \quad (7)$$

Because both instruments (i.e., at locations x and 0) were programmed with the same schedule, they turned on/off at the same time, thus producing time-series with the same timestamps and of the same length (i.e., same sample size). Therefore, for simplification, sample size was removed from the Eq. 7. Also note that each data point in the time-series of Eq. 7 represents a 3-s average.

Approach based on CDOM-correction

In a complex scenario, only the value of \bar{K}_w is constant and \bar{K}_g , \bar{K}_l , and \bar{K}_ϕ are not negligible and vary over time. In this case, it is necessary to obtain an independent time-series to separate the tracer and nonfilterable portions of $\bar{K}(x,t)$. For this study, the bivalves were assumed to filter all suspended particles whether they were phytoplanktonic or non-algal. Therefore, the attenuation coefficients, \bar{K}_ϕ and \bar{K}_l , were merged together into the attenuation coefficient for particles, \bar{K}_p , which was conceived as a proxy for the filterable tracer.

The values of $\bar{K}_p(x,t)$ were estimated by correcting $\bar{K}(x,t)$ for the attenuation due to CDOM and water (i.e., $\bar{K}_g(t)$ and \bar{K}_w). The value of \bar{K}_w was considered constant, but the value of $\bar{K}_g(t)$ was variable and dependent on the amount of CDOM-rich freshwater that was mixed in the mussel stratum, which was measured using in situ salinity from a conductivity sensor (2D-ACM; Falmouth Scientific), moored at mid-culture depth (4.5 m from the bottom) and approximately 15 m away from the TACCS inside the farm.

From the water samples, duplicate aliquots were sub-sampled to measure CDOM absorption and salinity. Samples were filtered through 0.2 μm membrane filters (Supore[®]-200, Gelman Scientific Laboratory) into 250 mL amber glass bottles with Teflon-lined caps and were transported on ice to the laboratory. Salinity was measured with a laboratory salinometer (AutoSal 8400B; Guildline Instruments).

The CDOM absorbance spectra from 275 to 850 nm were determined using a CARY 3 spectrophotometer (Varian) with a spectral resolution of 1 nm. Samples were scanned in 10 cm quartz cells using Nano-pure water as a reference. All glassware was acid-washed (24 h in a solution of 10% hydrochloric acid) and copiously rinsed with Nano-pure water. Approximately 5 min before sample scanning, sample bottles were transferred from the ice to a water bath to match the temperature inside the spectrophotometer ($\sim 27^\circ\text{C}$). The absorbance spectra were converted to absorptivity and corrected for scattering, index of refraction and blank drift following Johannsen and Miller (2001). The absorption coefficient at 490

nm, a_g , was estimated by averaging the coefficients between 488 to 492 nm.

An empirical linear algorithm was used to convert the time-series of in situ salinity [$S(t)$; dimensionless] into a time-series of absorption of CDOM [$a_g(t)$; m^{-1}]:

$$a_g(t) = m_g S(t) + n_g \quad (8)$$

where the coefficients m_g (m^{-1}) and n_g (m^{-1}) are the slope and intercept of the linear regression between salinity and a_g from the discrete water samples (Fig. 3b).

The estimated time-series of $a_g(t)$ was converted into a time-series of partial attenuation for CDOM, $\bar{K}_g(t)$, using the following modification of Eq. 2:

$$\bar{K}_g(t) = \frac{a_g(t)}{\bar{\mu}} \quad (9)$$

The involved simplifying assumptions were as follows: (1) The magnitude of the backscattering coefficient of CDOM (i.e., $b_{b,g}$; m^{-1}) was assumed negligible in comparison with the magnitude of a_g (Kirk 1994; Laanen et al. 2011). (2) The magnitude of $\bar{\mu}$ was assumed constant and equal to 0.7 (following Ciotti et al. 1999). (3) Salinity was assumed to be constant within the bivalve stratum and over the farm domain (after verification of CTD casts, data not shown).

The value of \bar{K}_w was estimated using the absorption coefficient of pure water from Pope and Fry (1997; 0.015 m^{-1} for 490 nm): $\bar{K}_w = a_w \bar{\mu}^{-1} = 0.0214 \text{ m}^{-1}$. The values of $\bar{K}_g(t)$ and \bar{K}_w were removed from the total attenuation measured with both TACCS to estimate the partial attenuation for particles, $\bar{K}_p(x,t)$:

$$\bar{K}_p(x,t) = \bar{K}(x,t) - [\bar{K}_g(t) + \bar{K}_w] \quad (10)$$

The ratio between the attenuation of particles inside the farm, $\bar{K}_p(x,t)$, and outside the farm, $\bar{K}_p(0,t)$, was used to calculate the instantaneous particle-based depletion index [$D_p(x,t)$; dimensionless], which approximates the fraction of particles remaining after mussel feeding at time t and at location x along the farm:

$$D_p(x,t) = \frac{\bar{K}_p(x,t)}{\bar{K}_p(0,t)} \quad (11)$$

Similarly to the Chl-based depletion index, the average particle-based depletion index ($\bar{D}_p(x)$; dimensionless) for location x along the current axis of the farm was calculated by dividing the average of the $D_p(x,t)$ data points by the average of the $D_p(0,t)$ data points:

$$\bar{D}_p(x) = \frac{\sum \bar{K}_p(x,t)}{\sum \bar{K}_p(0,t)} \quad (12)$$

Similarly to Eq. 7, the sample size of the two time-series was identical. Therefore, for simplification, it was removed from Eq. 12.

Assessment

General assessment (field application)

The proposed method (both approaches) was tested on two locations along the main current axis of the study farm (Fig. 1). To determine the main current axis of the farm, we used multiple deployments of a 2D-ACM current meter (Falmouth Scientific) over a period of approximately 1 month (data not shown). The main current axis approximated the 10 m isobath (see Fig. 1). The first location was close to edge of the farm (35 m into the farm) whereas the second location was approximately in the middle of the farm (300 m into the farm). Because we only had two TACCS instruments, we had to conduct our experiment in two phases. One TACCS was deployed outside the farm as a reference (see Fig. 1) during the two phases of the experiment. The second TACCS was deployed at the “edge” location from 19 to 21 Sep 2001 (i.e., phase 1), and then it was moved to the “mid-farm” location from 3 to 8 Oct 2001 (i.e., phase 2). The 12-day offset in the sampling events ensured that both locations were sampled during spring-tides (data not shown). Water samples used to calculate the empirical algorithm for the Chl: \bar{K} -regression approach (see Eq. 5; Fig. 3a) and the regression between absorption of CDOM and salinity for the CDOM-correction approach (Eq. 8; Fig. 3b)

were collected at times shown in Fig. 4c and Fig. 5c. Water samples were collected at the same time as the TACCS were collecting optical data (see water sampling section above).

In the edge location, the measured \bar{K} (mean \pm SD = $0.33 \pm 0.04 \text{ m}^{-1}$) and estimated Chl ($3.2 \pm 0.7 \text{ mg m}^{-3}$) were very similar (although differences were statistically significant; $P < 0.001$; $n = 1199$) to the values at the reference location ($\bar{K} = 0.35 \pm 0.04 \text{ m}^{-1}$; Chl = $3.4 \pm 0.9 \text{ mg m}^{-3}$; Fig. 4a and 4b). Consequently, the average depletion indices calculated using both, Chl: \bar{K} -regression (0.94) and CDOM-correction (0.95) approaches, showed weak seston gradients at the edge location (Fig. 4c and 4d).

In the mid-farm location, the measured \bar{K} ($0.35 \pm 0.03 \text{ m}^{-1}$) and estimated Chl ($3.4 \pm 0.6 \text{ mg m}^{-3}$) were significantly lower ($P < 0.001$; $n = 1007$) than the values at the reference location ($\bar{K} = 0.45 \pm 0.05 \text{ m}^{-1}$; Chl = $5.4 \pm 1.0 \text{ mg m}^{-3}$; Fig. 5a and 5b). As a consequence, the average depletion indices calculated using both Chl: \bar{K} -regression (0.63) and CDOM-correction (0.65) approaches showed that depletion at the mid-farm location was a lot stronger than at the edge-location (Fig. 5c and 5d).

Both \bar{K} and depletion time-series showed high variability that appeared to be related to interactions between tidal currents and bivalve suspension-feeding. The frequency distribution histograms of \bar{K} showed a bimodal distribution, proba-

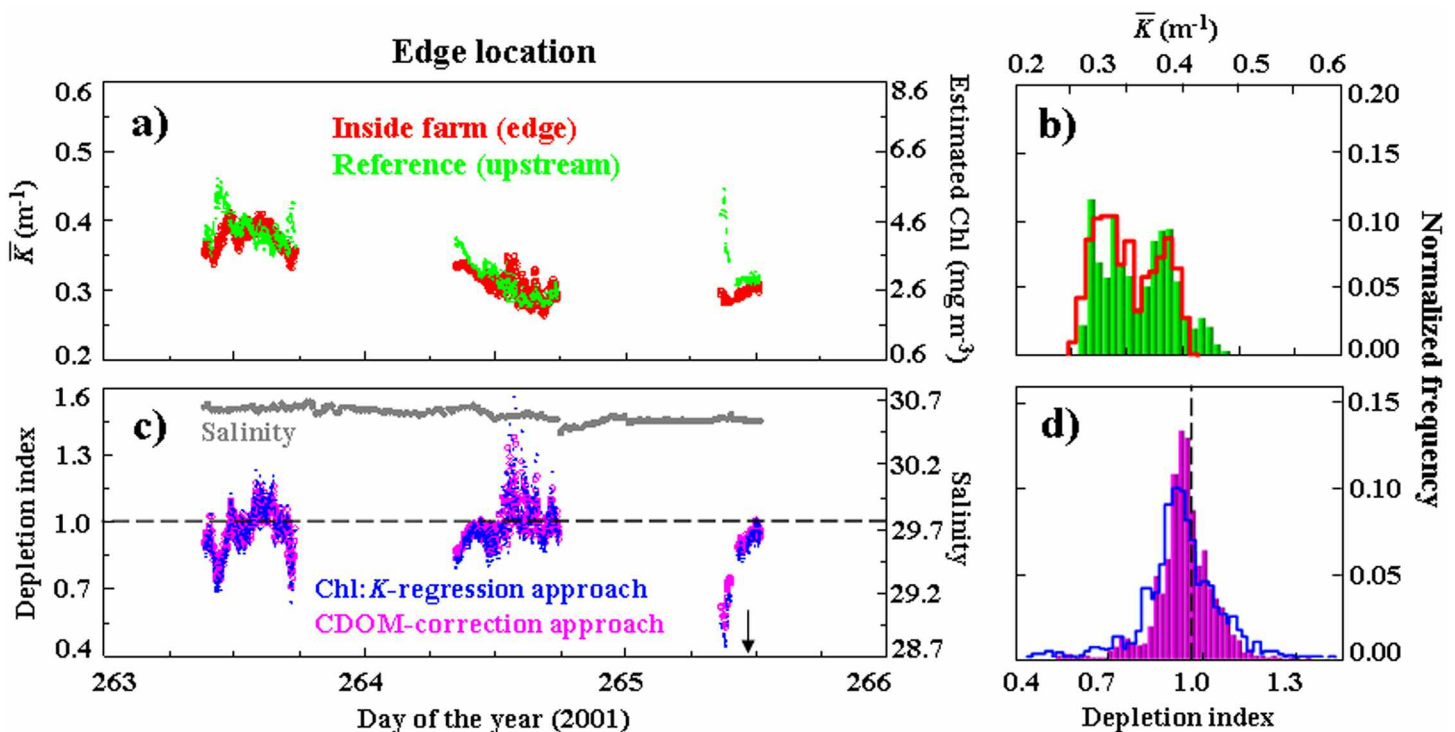


Fig. 4. Edge location ($n = 1199$). a) Time-series of the depth-averaged diffuse attenuation coefficient at 490 nm (\bar{K}) at the edge and reference locations (see Fig. 1). The estimated chlorophyll plus phaeopigments concentration (using Eq. 5) is shown in the right axis. b) Same data of a) represented as frequency distribution histograms. c) Time-series of the depletion index calculated with the Chl: \bar{K} -regression and CDOM-correction approaches. The dotted line represents no depletion. The time-series of salinity, used in the CDOM-correction approach (Eq. 8), is shown with respect to the right axis. Major ticks mark local midnight (GMT-3), and the arrow shows the time where water samples were collected. d) Same depletion data of c) represented as frequency distribution histograms. The dotted line represents no depletion.

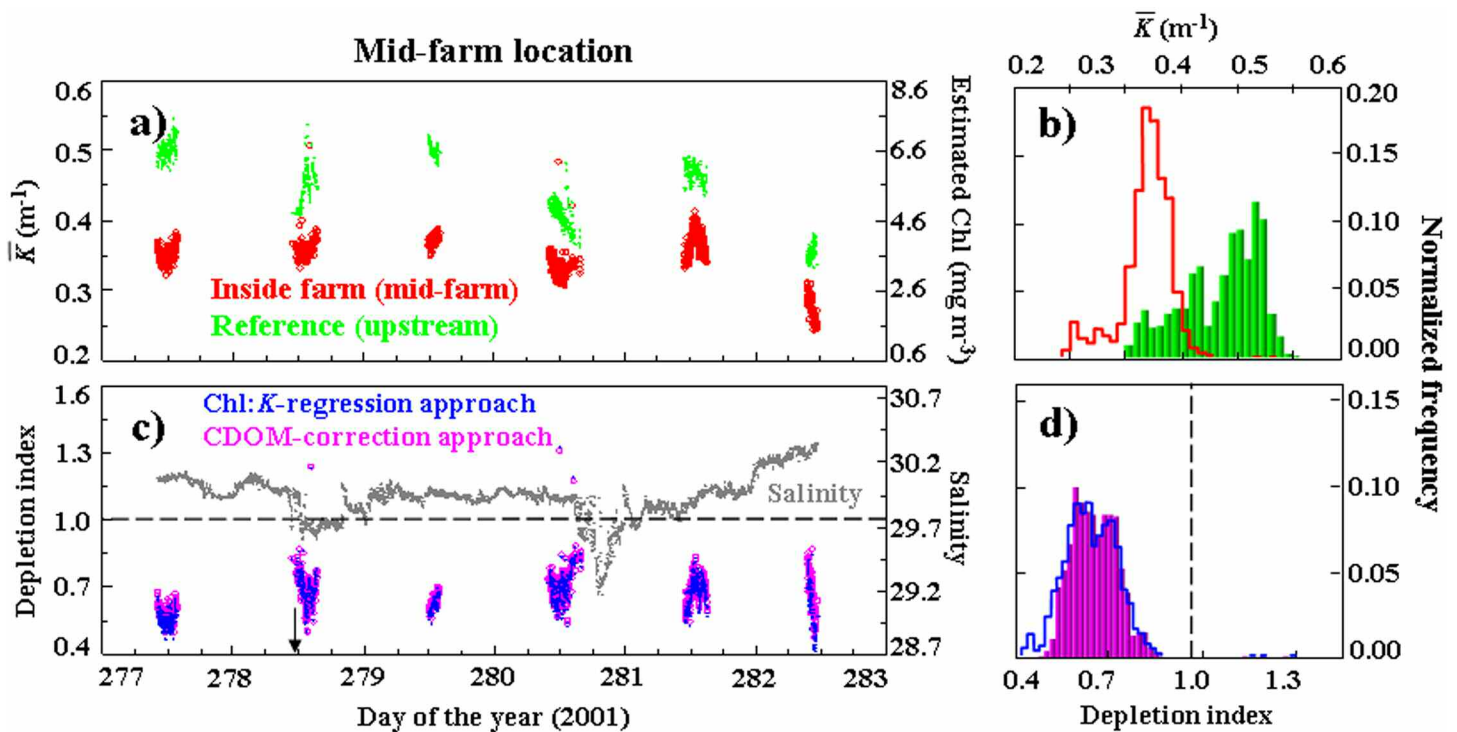


Fig. 5. Mid-farm location ($n = 1007$). Legend same as in Fig. 4.

bly associated with flood and ebb tides. However, the distribution histograms of depletion indices resembled a normal distribution. The observed high variability of \bar{K} is consistent with high tracer variability observed in other bivalve aquaculture sites (e.g., Heasman et al. 1998; Grant et al. 2008).

In conclusion, the presented method was tested in a real-world scenario and was successful at detecting statically significant time-averaged horizontal gradients of seston concentration. However, limitations that may prevent the application of this method under other conditions and in other environments are described below. The high variability of \bar{K} observed in this study supports the idea that previous studies were not able to find statistically significant gradients of seston because of limitations in the temporal and/or vertical resolution of their employed methods.

Offset estimation (approach comparison)

To achieve a robust estimation of the depletion index, it is critical to accurately estimate the offset due to the concentration of nonfilterable light-attenuating substances, or in other words, to accurately estimate the *true* (and unknown) value of \bar{K} at zero tracer concentration. In this study, attenuation by nonfilterable substances was estimated empirically (n_{Chl} ; *Chl*: \bar{K} -regression approach) and semi-analytically ($\bar{K}_g + \bar{K}_w$; CDOM-correction approach). Both approaches were independent attempts to estimate the *true* value of \bar{K} in the absence of tracer. Discrepancies between the estimated offset (i.e., n_{Chl} or $\bar{K}_g + \bar{K}_w$) and the *true* offset will result in spurious estimations of the depletion index. The mathematical reason

for this effect can be inferred from Eqs. 5 and 6. If the coefficients from Eq. 5 are assumed to be the same inside and outside the farm, then the slope m_{Chl} for inside and outside the farm will cancel each other out in Eq. 6, making evident that depletion index depends solely on n_{Chl} , the value of \bar{K} when *Chl* is zero.

The effect that incorrect estimations of the *true* offset has on the *measured* depletion index (i.e., D') was modeled by changing n_{Chl} in Eq. 6 by know percentages ranging from 90% underestimation to 90% overestimation of the *true* n_{Chl} . The model was initialized with the average $\bar{K}(x,t)$ measured in this study and with the empirical n_{Chl} estimated for this study. The modeled results (Fig. 6) show that the *measured* depletion index is not very sensitive to spurious estimations of the *true* offset at levels of depletion between 0.5 and 1.5. For example, a 10% overestimation of the *true* offset will lead only 2% underestimation of the *measured* depletion index at an average D of 0.8.

For this study, we first verified that the offset calculated with the *Chl*: \bar{K} -regression approach (i.e., n_{Chl}) was approximately constant over the study period by comparing the depletion indices calculated with the approach that assumed a constant offset (D_{chl}), against the indices estimated with the approach that allowed a variable offset (D_p). Once the assumption of a constant offset was confirmed, the accuracy of the estimated offset was assessed by comparing the empirical algorithm determined statistically with the *Chl*: \bar{K} -regression approach, against an expected theoretical relationship.

In Fig. 6, the particle-based depletion index (D_p) was com-

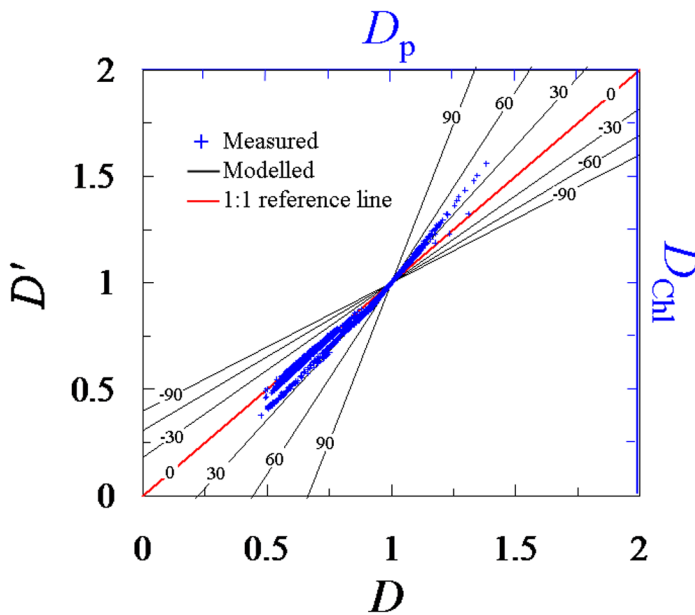


Fig. 6. Black lines and axis: Modeled measured depletion indices (i.e., D') against known *true* depletion indices (i.e., D) for several percentages of overestimation (positive values) and underestimation (negative values) of the *true* offset due to nonfilterable substances (i.e., n_{chl}). Blue crosses and axis: Measured depletion indices calculated with the *Chl*: \bar{K} -regression approach (i.e., D_{chl}) against depletion indices calculated with the CDOM-correction approach (i.e., D_p).

pared with the *Chl*-based depletion index (D_{chl}). The values of D_{chl} exhibited approximately a 1-to-1 relationship with respect to the values of D_p (Fig. 6, slope = 0.9, $R^2 = 0.99$, $n = 2206$). The small average difference between D_{chl} and D_p ($3 \pm 3\%$) suggest that, for this study, the assumption of a constant offset was valid. However, the application of the *Chl*: \bar{K} -regression approach may not be valid in environments where CDOM is more variable and has a stronger contribution to \bar{K} .

The algorithm determined empirically using the *Chl*: \bar{K} -regression approach ($\bar{K} = 0.052 \text{ Chl} + 0.167$; $R^2 = 0.99$; $n = 4$; Fig. 3a), was compared with the following expected theoretical relationship (from Eq. 2 and 3):

$$\bar{K} = \frac{a_{\phi}^* + b_{b,\phi}^*}{\bar{\mu}} \text{Chl} + (\bar{K}_w + \bar{K}_g + \bar{K}_t) \quad (13)$$

where a_{ϕ}^* ($\text{m}^2 \text{ mg}^{-1}$) and $b_{b,\phi}^*$ ($\text{m}^2 \text{ mg}^{-1}$) are the specific absorption and backscattering coefficients of phytoplankton, respectively. The value of $b_{b,\phi}^*$ is usually a lot smaller than the value of a_{ϕ}^* , which can vary from $0.01 \text{ m}^2 \text{ mg}^{-1}$ for microplankton to $0.04 \text{ m}^2 \text{ mg}^{-1}$ for picoplankton (Ciotti et al. 2002). Assuming negligible $b_{b,\phi}^*$ and an average value of a_{ϕ}^* of $0.03 \text{ m}^2 \text{ mg}^{-1}$, the theoretical slope, $a_{\phi}^* \bar{\mu}^{-1}$, would be $0.043 \text{ m}^2 \text{ mg}^{-1}$, which is similar to the value of the statistically determined slope (i.e., $m_{chl} = 0.052 \text{ m}^2 \text{ mg}^{-1}$). Moreover, if we compare the theoretical intercept accounting only for the attenuation of water and CDOM (i.e., $\bar{K}_w + \bar{K}_g = 0.144 \text{ m}^{-1}$) against the intercept determined statistically ($n_{chl} = 0.167 \text{ m}^{-1}$), we can infer

that the attenuation due to non-algal particles was relatively small (i.e., $\bar{K}_t = 0.023 \text{ m}^{-1}$). As mentioned before, the difference between the calculated and the theoretical slopes has no influence in the estimated depletion index. Moreover, the 16% overestimation of the statistically determined intercept, n_{chl} , lead to only 3% underestimation of the calculated depletion index when compared against the depletion calculated with the theoretical intercept, $\bar{K}_w + \bar{K}_g = 0.144 \text{ m}^{-1}$.

In conclusion, if the coefficients of the linear regression between \bar{K} and tracer concentration outside the farm (i.e., m_{chl} and n_{chl}) are equal to the coefficients inside the farm (a reasonable assumption when the outside and inside locations are within a few hundred meters of each other), the value of the slope (m_{chl}) has no influence on the *measured* depletion index (D) and the value of the offset (n_{chl}) has little influence on D for indices between 0.5 and 1.5. However, for depletion indices < 0.5 or > 1.5 , errors larger than 40% on the estimated n_{chl} can lead to unacceptable (i.e., $> 20\%$) errors in the *measured* depletion index. For this study, the assumption of a constant offset was a reasonable approximation and the error in D due to offset estimation was negligible.

Effect of the average cosine

As expressed in Eq. 2, the value of \bar{K} depends on the average cosine for downwelling irradiance, $\bar{\mu}$, which is a parameter that represents the angular distribution of downwelling photons at a given point in the underwater field (Kirk 1994). The value of $\bar{\mu}$ at the sea surface depends primarily on sun angle and cloud coverage (e.g., Zheng et al. 2002). In the water column however, scattering of photons cause $\bar{\mu}$ to decrease exponentially with depth up to an asymptotic value (Berwald et al. 1995; Piening and McCormick 2003). Both, the rate of decrease and the asymptotic value of $\bar{\mu}$, depend on the b/a ratio (Kirk 1994). The effect of $\bar{\mu}$ on the *measured* depletion index, D' , was assessed by substituting K from Eq. 2 into Eq. 11:

$$D'(x) \approx \frac{[a_p(x) + b_{b_p}(x)]\bar{\mu}(0)}{[a_p(0) + b_{b_p}(0)]\bar{\mu}(x)} \quad (14)$$

It is evident from the above equation that the calculated depletion index is not affected by the light field distribution as long as the average cosine outside the farm, $\bar{\mu}(0)$, is equal to the average cosine inside the farm, $\bar{\mu}(x)$. Because \bar{K} inside and outside the farm were measured at the same depth and under almost identical surface illumination conditions; depth, sun angle, and cloud cover were likely to cause negligible changes between $\bar{\mu}(0)$ and $\bar{\mu}(x)$. However, bivalve suspension-feeding can cause changes in the b/a ratio of the medium by selectively removing scattering particles (i.e., phytoplankton, detrital, and mineral particles). If the b/a ratio decreases, the value of $\bar{\mu}(x)$ could increase [with respect to $\bar{\mu}(0)$] and the *measured* depletion index could spuriously decrease.

We conducted a sensitivity analysis to assess the effect of variations in the b/a ratio due to suspension-feeding on the

measured depletion index, D' (Fig. 7). Four scenarios were tested where seston was composed exclusively by phytoplankton or mineral particles in waters with high or low CDOM. The parameters used to define boundary conditions at the reference site are shown in Table 2. For each scenario, the IOPs of particles at the reference site [i.e., $a_p(0)$, $b_p(0)$ and $b_{bp}(0)$] were used to calculate the IOPs of particles at the location inside the farm [i.e., $a_p(x)$, $b_p(x)$ and $b_{bp}(x)$] for a range of true depletion indices varying from 0 to 2 [e.g., $a_p(x) = a_p(0) \times D(x)$]. Suspension-feeding by bivalves was assumed to affect only particles, hence the IOPs of water and CDOM at the inside-farm location [i.e., a_w and $a_g(x)$] were equal to the IOPs at the reference location. Once the matrix of IOPs were completed for all the given true depletion indices, the total absorption, scattering and backscattering coefficients (i.e., a , b and b_b , respectively) were calculated as the sum of all partial absorption, scattering and backscattering coefficients of the medium,

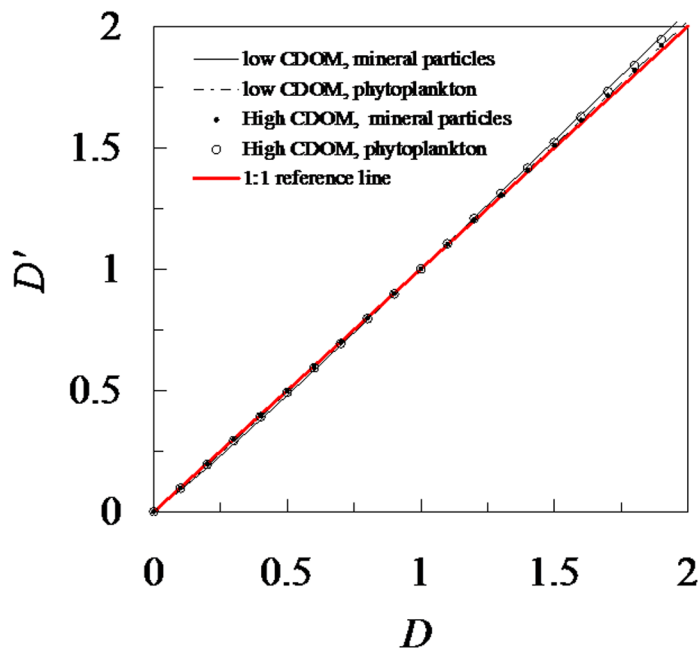


Fig. 7. Relationship between true depletion indices (i.e., D) and depletion indices modeled under varying average cosine for downwelling irradiance (i.e., D'), according to four contrasting scenarios (see details in text).

Table 2. IOPs used in the sensitivity analysis to assess the effect of $\bar{\mu}$ on D .

(490 nm) m^{-1}				
a	b	b_b	Reference	
Phytoplankton	0.1	0.3	0.00001	Green and Sosik 2004
Mineral particles	0.025	0.1	0.004	Green and Sosik 2004
Low CDOM	0.001	0	0	Blough et al. 1993
High CDOM	0.5	0	0	Blough et al. 1993
Water	0.015	0	0	Pope and Fry 1997

respectively. The value of $\bar{\mu}(x)$ for all the given true depletion indices was calculated from the b/a ratio using Fig. 6.16 in Kirk (1994) and the measured depletion indices were calculated using Eq. 14.

The values for the IOPs chosen for the different scenarios of the analysis resulted in b/a ratios in the range of 0 to 3, which is the range where $\bar{\mu}$ is most sensitive to changes in the b/a ratio (i.e., $\bar{\mu}$ rapidly changes from 1 to 0.83). Therefore, the results of our sensitivity analysis are representative of the worst case scenario.

The results of the sensitivity analysis (Fig. 7) show that the measured depletion index, D' , is not sensitive to changes in $\bar{\mu}$ due to variations in the b/a ratio caused by bivalve suspension-feeding. The maximum average error in D (3%) occurred in the scenario where seston was composed exclusively of mineral particles with high backscattering coefficient, on water with low CDOM. Although measurements of \bar{K} can be strongly influenced by $\bar{\mu}$ (e.g., Zheng et al. 2002), measurements of depletion index are not.

In conclusion, a negligible effect of the angular distribution of the underwater light field may be assumed while assessing horizontal gradients of seston using multiple moorings with sensors at the same depth and under approximately equal surface illumination conditions.

Effect of spurious irradiances (biofouling and frame-shading)

The film of biofouling that accumulates over the irradiance sensors, the shade created by the frame around TACCS and errors in sensor calibration, can artificially modify the measured E on the vertical sensor array, which could result in errors in the calculated \bar{K} and D .

Effect on \bar{K}

If we define \bar{K}' as the value of attenuation measured with sensors that were subject to some degree of biofouling, frame-shading, and/or calibration error, then:

$$\bar{K}' = \frac{-\ln\left(\frac{E(z_L) - [E(z_L) \times \beta(z_L)]}{E(z_U) - [E(z_U) \times \beta(z_U)]}\right)}{z_L - z_U} \quad (15)$$

where $\beta(z)$ is the proportion of change in irradiance on a sensor at depth z , associated with biofouling, frame-shading, and/or calibration errors (i.e., $\beta(z) = [E(z) - E'(z)] E(z)^{-1}$; dimen-

sionless). If we consider \bar{K} as the *true* value of attenuation calculated (from Eq. 4) in the absence of biofouling, shading, or any other artificial modifier of E , then:

$$\bar{K} = \bar{K}' - \frac{-\ln\left(\frac{1-\beta(z_L)}{1-\beta(z_U)}\right)}{z_L - z_U} = \bar{K}' - \bar{\kappa} \quad (16)$$

where $\bar{\kappa}$ (m^{-1}) is the attenuation coefficient spuriously increased (or decreased) due to biofouling, frame-shading, or calibration errors. It is evident from this equation that if $\beta(z_U) = \beta(z_L)$, then $\bar{\kappa} = 0$ and the *measured* attenuation is equal to the *true* attenuation (i.e., $\bar{K}' = \bar{K}$). It is also important to emphasize that increasing the distance between the two irradiance sensors of the vertical array (i.e., $z_L - z_U$) will tend to decrease the magnitude of $\bar{\kappa}$, making the estimation of \bar{K} more robust.

The fraction of irradiance reduced due to one-week accumulated biofouling was assessed on 17 Aug 2001. Sensors from the vertical array at 4 and 8 m were held together pointing the zenith and were allowed to record continuously for approximately 10 s. The thin layer of biofouling that was accumulated throughout the week was cleaned using a moist microscope-grade tissue paper. Care was taken to clean sensors without changing their orientation to minimize changes in the measured irradiances that were not due to biofouling. The proportion of change in E associated with biofouling was $\beta(z_4) = 0.03$ and $\beta(z_8) = 0.05$ and the corresponding value of $\bar{\kappa}$ (calculated with Eq. 16) was 0.005 m^{-1} , which only represents a 1% reduction of the average \bar{K}' measured in this study.

We also assessed the effect of frame-shading on \bar{K} by comparing measurements of TACCS (with frame) against \bar{K} measured with a free-falling profiling radiometer (SPMR; Satlantic). The use of profiling radiometers is the traditional and most widely used method to calculate \bar{K} (see reviews by Morel 1998 and Morel and Maritorena 2001). On seven occasions between 21 Sep and 16 Oct 2001, the SPMR profiler was deployed at approximately 15 m away from TACCS. The attenuation coefficient, \bar{K} , was calculated by fitting the vertical irradiance profiles measured with the profiler to the following equation:

$$E(z, x, t) = E(z_U, x, t)e^{-\bar{K}(x,t)(z-z_U)} \quad (17)$$

The value of $E(z_U, x, t)$ is the irradiance at the upper boundary of the bivalve stratum (4 m from the surface) and the values of $E(z, x, t)$ are the irradiances at increasing depths up to the lower boundary of the bivalve stratum (8 m). A surface irradiance reference was not used because the entire water column was typically profiled in < 10 s. Therefore, surface irradiance was assumed constant throughout each profiling exercise. Profiles had 71 ± 8 data points within the bivalve stratum and fits to Eq. 17 were always with $R^2 > 0.99$. The values of \bar{K} measured with TACCS were, on average, 4% higher than the \bar{K} measured with the profiling radiometer ($R^2 = 0.98$, $n = 7$, $P < 0.01$, Fig. 8).

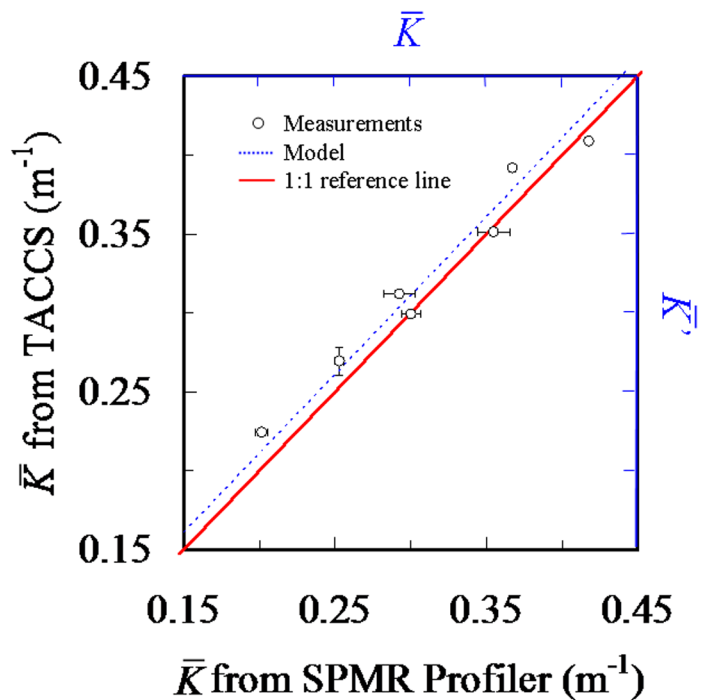


Fig. 8. Black circles and axis: Values of the diffuse attenuation coefficient at 490 nm (i.e., \bar{K}) measured with TACCS against measurements of \bar{K} measured with the SPMR profiling radiometer. Blue line and axis: Relationship between the *measured* (i.e., \bar{K}') and *true* (i.e., \bar{K}) attenuation coefficients modeled with parameters chosen to simulate frame-shading estimated for this study (i.e., $\beta(z_4) = 0.12$ and $\beta(z_8) = 0.08$).

This small yet spurious increase in \bar{K} was also modeled using Eq. 16 and estimations of $\beta(z_U)$ and $\beta(z_L)$ from measurements of \bar{K} from 23 Aug 2001. One TACCS was kept inside the frame while the other TACCS was positioned 15 m away with no frame. Both instruments logged continuously from 1205 to 1239 hours and 1-min averages were calculated. During the experiment, the sky was free of clouds and the sea surface had small ripples. The measured reductions in E , $\beta(z_4) = 0.12$ and $\beta(z_8) = 0.08$ (for both $P < 0.001$, $n = 35$), were used in Eq. 16 to compute \bar{K}' over the range measured with the SPMR profiler (Fig. 8, blue line). The average modeled \bar{K}' was 3% higher than the *true* \bar{K} , and was consistent with the spurious increase in \bar{K} measured with the SPMR profiler.

In conclusion, spurious reductions in the measured irradiance due to 1 week of biofouling and frame-shading were likely to cause only minor errors in the \bar{K} calculated in the present study. However, biofouling may cause larger errors during longer deployments or in regions subject to heavier biofouling. Moreover, frame-shading may have a larger effect if the E sensors are closer to the frame or if a bigger frame is used. It is recommended to routinely estimate the β and $\bar{\kappa}$ coefficients during sensor cleaning to verify the magnitude of the errors due to biofouling. If biofouling is not negligible, time-series of $\beta(z, t)$ can be used (in Eq. 16) to correct the time-series of E for the effect of biofouling. Methods to reduced bio-

fouling on sensors, such as the use of shutters and copper, should be considered to increase the length of deployments and to reduce the effect of biofouling (see Manov et al. 2004). It is also recommended to estimate the β and $\bar{\kappa}$ coefficients associated with frame-shading, under different surface illumination conditions, every time that a new instrument configuration is employed. The effect of instrument shading on upwelling radiance and irradiance (for the calculation of remote sensing reflectance) has been studied in field experiments and using Monte Carlo simulations (Aas and Korsbo 1997; Piskozub 2004), but the effect of shading on downwelling irradiance (for the calculation of diffuse attenuation coefficients) has not been studied extensively.

Effect on D

We assessed the effect of spurious changes in irradiance on the depletion index calculated with the *Chl*: \bar{K} -regression approach, D_{chl} . However, the following reasoning also applies for the D_p .

If the *true* depletion index is defined as in Eq. 6, and the depletion index *measured* under the effect of biofouling, frame-shading, and/or calibration errors is $D'(x) = [\bar{K}'(x) - n_{chl}] [\bar{K}'(0) - n_{chl}]^{-1}$, then the *true* depletion index can be expressed in terms of the *measured* \bar{K}' (from Eqs. 6 and 16) as:

$$D(x) = \frac{[\bar{K}'(x) - n_{chl}] - \bar{\kappa}(x)}{[\bar{K}'(0) - n_{chl}] - \bar{\kappa}(0)} = \frac{D'(x)[\bar{K}'(0) - n_{chl}] - \bar{\kappa}(x)}{[\bar{K}'(0) - n_{chl}] - \bar{\kappa}(0)} \quad (18)$$

We used the above equation to assess the sensitivity of D' to spurious changes in irradiance due to biofouling, frame-shading, and calibration errors (Fig. 9). Three scenarios were tested and the $\beta(z, x)$ parameters for each scenario are shown in the table in Fig. 9. The first scenario simulated the effect of the frame used in this study; hence irradiance was reduced by 12% in the upper sensors and by 8% in the lower sensors (following the results shown above). This algorithm was also applied to the $\bar{K}'(x)$ and $\bar{K}'(0)$ measured in this study to obtain an estimate of the *true* depletion (see Fig. 9, blue crosses). The second scenario was designed to assess the effect of vertical changes of β (i.e., upper sensors with respect to lower sensors), hence the reduction of irradiance in the upper sensors was increased by a factor of 3, simulating either the effect of bigger frames, or the effect of frame-shading plus homogeneous biofouling (i.e., equal outside and inside the farm). The third scenario was designed to assess the effect of horizontal changes of β (i.e., inside sensors with respect to outside sensors), therefore the reduction of irradiance in the inside sensors was increased by a factor of 3, simulating the effect of different frames and/or heterogeneous biofouling (i.e., different inside and outside the farm). The average \bar{K} and the estimated n_{chl} for this study were used in all three scenarios. For each of the three scenarios, Eq. 18 was used to estimate the *measured* depletion, D' , for a range of *true* depletion indices varying from 0 to 2 (Fig. 8).

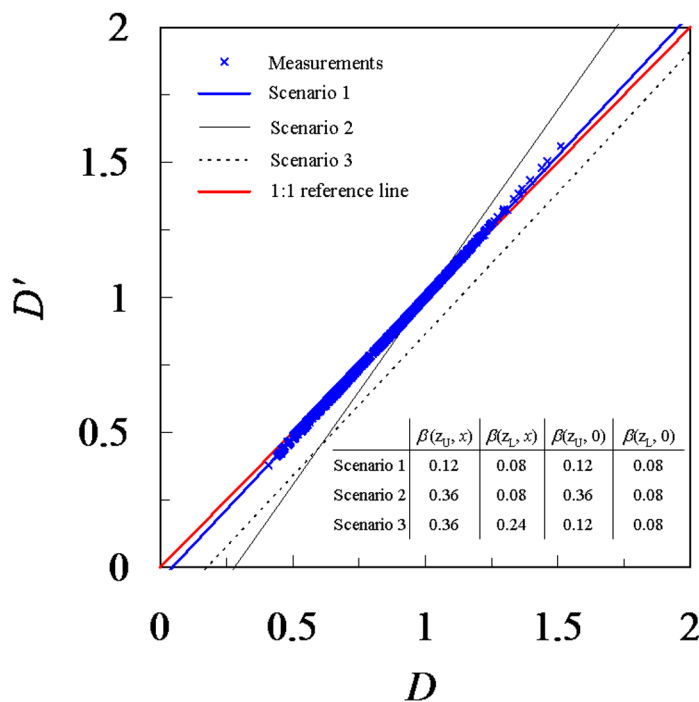


Fig. 9. Relationship between depletion indices measured under the effect of biofouling, frame-shading, and/or calibration errors (i.e., D') and the *true* depletion indices (i.e., D) modeled for three scenarios. Parameters used in the three scenarios are shown in the table.

The results from the sensitivity analysis (Fig. 9) show that the *measured* depletion is not very sensitive to errors in the *measured* irradiance due to biofouling, frame-shading, and sensor calibration. For the range of depletion measured in this study, the *measured* depletion underestimated the *true* depletion by $1.2 \pm 1.3\%$ according to parameters used in scenario 1. Moreover, a vertical increase of β by a factor of 3 resulted in a decrease of the *measured* depletion by a factor of 0.97 and a horizontal increase of β by a factor of 3 resulted in a decrease of the measured depletion by a factor of 0.94.

Vertical changes of β (i.e., upper sensors with respect to the lower sensors) modify the slope of the $D:D'$ regression; while horizontal changes of β (i.e., inside sensors with respect to outside sensors) modify the intercept of the $D:D'$ regression. Therefore, vertical changes of β have a greater effect on *measured* depletion indices $\ll 1$ and $\gg 1$ and little effect on *measured* depletion indices of ~ 1 , whereas horizontal changes of β have the same effect on all *measured* depletion indices. Vertical changes of β have the same effect as spurious estimations of n_{chl} the offset due to non-tracer substances (described before).

In conclusion, spurious reductions in the measured irradiance due to biofouling and frame-shading, and/or sensor calibration errors had little effect on the depletion indices calculated in the present study. However, cases with larger errors in the measured irradiance at sites with strong seston gradients (e.g., $D \ll 1$) may prevent accurate estimation of the depletion

index. As mention before, it is important to estimate the β and $\bar{\kappa}$ coefficients associated with biofouling and frame-shading.

Effect of wave focusing

Surface waves refract sunlight causing focusing and defocusing of direct sunlight that can cause strong fluctuations in the measured E (Zaneveld et al. 2001). The effect of wave-focusing on the variability of the measured \bar{K} was assessed between 1 Aug and 5 Sep 2001. Although TACCS were programmed to sample for 3 s every minute, TACCS were also programmed to extend the sampling period to 20 s on the first minute of every hour. The coefficient of variation of \bar{K} calculated for those extended 20 s sampling periods ($n = 25,308$) were 30.5% for $\bar{K}(z_1 \rightarrow z_2)$, 7.3% for $\bar{K}(z_2 \rightarrow z_4)$, and 1.1% for the bivalve stratum [i.e., $\bar{K}(z_4 \rightarrow z_8)$]. Wave focusing causes an increase of variability in the measured \bar{K} . However, such variability decreased with depth.

To obtain robust estimations of \bar{K} , it is recommended to obtain continuous measurements of \bar{K} , over a period of several seconds, to record several cycles of sunlight focusing and defocusing caused by waves of different periods. This will be particularly important when the assessed bivalve stratum is close to the surface. The irradiance distribution may depart from normality depending on cloud cover, sun angle, and depth. Therefore, we recommend calculating medians as a descriptor of central tendency of irradiance. In this study, the E sensors at the bivalve stratum were sufficiently distant from the surface to result in relatively low coefficient of variation of \bar{K} .

Sediment resuspension

The proposed method assumes that the filterable tracer has a conservative nature (i.e., negligible production or loss of tracer particles within the farm due to processes other than bivalve feeding). This assumption can be violated during sediment-resuspension events, which are common in high wind situations in coastal regions (see Pilditch et al. 2001). If sediments are resuspended high enough from the sea floor, they could enter the bivalve stratum (from underneath) increasing both, $\bar{K}(0,t)$ and $\bar{K}(x,t)$, and causing spurious estimations of both, D_{chl} and D_p depletion indices. If resuspension of sediments occurs with the same intensity at the inside and reference locations, the effect of sediment resuspension on the *measured* depletion index will be equivalent to an underestimation of the *true* offset, as explained in the previous section (Fig. 6). If there is more resuspension of sediments at one of the two locations (i.e., heterogeneous resuspension), the effect on the *measured* D will be equivalent to the effect of horizontal changes of β due to different frame sizes and/or heterogeneous biofouling.

Continuous measurements that are water-column integrated and that are a proxy for nonalgal particles are required to correct for the effect of sediment resuspension. Measurements of diffuse attenuation at multiple wavelengths may be a suitable mean to resolve for non-algal particle concentration (Dickey 2003). However, if a significant proportion of the

resuspended material is algal in nature (e.g., benthic diatoms), then multi-spectral attenuation (or any other chlorophyll-sensing instrument) cannot be used to correct for resuspension. However, continuous measurements of turbidity from transmissometers and backscatter meters can help to flag times when resuspension occurred if deployed beside the lower sensors of the E vertical array.

In this study, continuous measurements of turbidity were not available. Therefore, the presence of resuspended sediments was only assessed seven times between 21 Sep and 16 Oct 2001. Three 400 mL aliquots were filtered onto pre-ashed and pre-weighed Whatman GF/F glass fiber filters. Filters were rinsed with 10 mL of an isotonic solution of ammonium formate to remove salts. Filters were transported on dry ice to the laboratory, dried 24 h at 65°C and combusted 5 h at 450°C (see details in Cranford and Hargrave 1994). The POM/PIM ratio of the water samples was compared with wind speed data from a weather station (Weather Wizard III, Davis Instruments) mounted 500 m away from the study farm. The POM/PIM ratios suggested that sediment resuspension (i.e., POM/PIM < 2) occurred at wind speeds of 24 km h⁻¹ but not at wind speeds < 19 km h⁻¹. Only 8% of the in situ wind speed data points occurred at wind speeds > 19 km h⁻¹ suggesting that, given the site, depth, and weather conditions of this study, sediment resuspension did not play an important role during this experiment. However, studies conducted in shallower environments, or in conditions where sediments resuspension events play a more important role, would need to employ independent measurements of turbidity to correct for sediment resuspension.

Production of faeces and pseudo-faeces

Underestimation of the depletion index could occur if a significant part of \bar{K} is attributed to bivalve biodeposits (faeces and pseudofaeces). On average however, the contribution of biodeposits to \bar{K} is believed to be at least 100 times smaller (see calculations below) than the contribution of prefiltered seston because (1) seston reworked by bivalves is repacked into pellets, (2) seston ingested by bivalves is subjected to digestion, which degrades pigments and reduces their ability to absorb light, and (3) the amount of seston in the form of biodeposits is limited by the amount of prefiltered seston.

Seston pelletization

Seston exposed to bivalve suspension-feeding is repacked into pellets (Bayne et al. 1993). Pellets can be discarded before ingestion (i.e., pseudofaeces) or after ingestion/digestion (i.e., faeces). In either case, the surface:volume ratio of the pellets is reduced with respect to seston before filtration. Seston weight is proportional to its volume, and seston light attenuation is proportional to its surface. Therefore, seston pelletization should reduce its efficiency to attenuate light. The effect of particle size and geometry on the bulk optical properties has been studied experimentally, and predicted using Mie theory, for a variety of phytoplankton taxa (Morel and Bricaud 1986). However, there are no studies regarding the optical properties

of bivalve biodeposits. A first order approximation of the effect of seston pelletization on \bar{K} can be inferred from the relationship between the IOPs and particle geometry (following Morel and Bricaud 1986):

$$a = sQ_a \left(\frac{N}{V} \right) \quad (19)$$

and

$$b_b = sQ_b \left(\frac{N}{V} \right) \quad (20)$$

where N is the number of particles in a solution of volume V , the parameter s is the cross-sectional area and the parameters Q_a and Q_b are the efficiency factors for absorption and backscattering, respectively.

The ratio of diffuse attenuation of particles in a solution of volume V (i.e., \bar{K}_p) to the diffuse attenuation of the same material packed into one seston pellet (i.e., \bar{K}_Π) can be assessed rearranging Eqs. 2, 19, and 20:

$$\frac{\bar{K}_p}{\bar{K}_\Pi} = \frac{\left[s_p Q_{a_p} \left(\frac{N_p}{V} \right) + s_p Q_{b_p} \left(\frac{N_p}{V} \right) \right] \bar{\mu}_p^{-1}}{\left[s_\Pi Q_{a_\Pi} \left(\frac{1}{V} \right) + s_\Pi Q_{b_\Pi} \left(\frac{1}{V} \right) \right] \bar{\mu}_\Pi^{-1}} \quad (21)$$

Assuming that (1) the efficiency factors are the same for seston in particles and seston in a pellet, (2) all seston particles have the same size, (3) seston particles and the pellet have a spherical shape, and (4) differences between $\bar{\mu}_p$ and $\bar{\mu}_\Pi$ are negligible compared with the differences between s_p and s_Π , Eq. 21 can be expressed as:

$$\frac{\bar{K}_p}{\bar{K}_\Pi} \approx \frac{r_\Pi}{r_p} \quad (22)$$

where, the value of r_p is the equivalent radius of a phytoplankton typical of coastal ecosystems (i.e., 5×10^{-6} m; Morel and Bricaud 1986), and r is the equivalent radius of a faecal pellet (approximately 5×10^{-4} m). Therefore, \bar{K}_Π will be at least 100 times smaller than \bar{K}_p . It is important to emphasize that these are the most conservative estimates and that violations of the involved assumptions will increase the $\bar{K}_p : \bar{K}_\Pi$ ratio, making our argument stronger. Biodeposit-pellets are "invisible" to TACCS with respect to seston before bivalve filtration.

Seston digestion

After ingestion, the digestion process removes (or degrades) most of the photosynthetic primary pigments that give phytoplankton its characteristic color. Kotta and Møhlenberg (2002) observed that approximately 64% (by weight) of Chl *a* and phaeophorbide *a* are lost in the guts of the mussel *M. edulis*. Although there have not been any studies describing the absorption spectra of bivalve biodeposits, it is expected that the absorption spectra of bivalve faeces resemble more the spectra

of detritus than the spectra of phytoplankton. Seston subject to bivalve filtration and digestion is not likely to be as efficient at absorbing light at 490 nm as predigested seston.

Biodeposit abundance

Regardless the probable low light attenuation efficiency of biodeposits, if faeces concentration is a lot greater than the concentration of prefiltered seston, spurious estimations of D could occur. However, once seston is filtered from the water column by bivalves, a fraction is retained in the form of tissue or shell, a fraction is excreted or respired in the form of dissolved nutrients, and the rest returns to the seston pool in the form of faeces and pseudofaeces (e.g., Pouvreau et al. 2000). Therefore, the average concentration of biodeposits should be less than the average concentration of prefiltered seston. However, faeces and pseudofaeces may not return to the water column immediately after production; instead they can be accumulated in the interstitial spaces of the conglomerate of bivalves along the ropes. The accumulated biodeposits may not return to the water column until the ropes are disturbed by currents induced by high winds. Therefore, the instantaneous concentration of biodeposits may be greater than the instantaneous concentration of prefiltered seston during high wind events. In this case, the assumption of a conservative tracer will be violated causing spurious estimations of the depletion index as explained in the section of sediment resuspension. The suggested means to detect and to correct for sediment resuspension also apply for the detection and correction of resuspension of biodeposits from the mussel ropes.

Changes in seston size-distribution

As mentioned before, light attenuation depends on the surface:volume ratio of the particles in the medium (Morel and Bricaud 1986). Therefore, the magnitude of \bar{K} is dependent on the seston size-distribution. Processes such as seston aggregation (i.e., production of flocs) or seston disaggregation will result in changes of \bar{K} that are not related to seston depletion by bivalve suspension-feeding. The implicit assumption of the proposed method is that the seston size-distribution remains constant throughout the farm domain. If seston in the outside location is organized in aggregates and these flocs break up while being transported to the inside location, the calculated depletion index will be underestimated. On the contrary, if seston is aggregated in flocs before arriving to the inside location, the calculated depletion index will be overestimated. Floc dynamics within bivalve farms have not been studied, and whether seston aggregates or disaggregates as a consequence of interactions with cultured organisms and gear, is not clear.

Production of CDOM

CDOM can be produced in sediments (e.g., Shank et al. 2005). Because sediments (mainly faeces and pseudo-faeces) often accumulate in the interstitial spaces among the bivalves, there is the possibility that CDOM can be produced from these sediments on the bivalve lines. This production of CDOM would covary with the depletion of phytoplankton and could

lead to an underestimation of the Depletion index. The *instruments* used in this study operate at 490 nm: a wavelength where CDOM has a relatively small influence. However, to improve the accuracy of this method, it is recommended to use additional data (e.g., multi-spectral \bar{K} or a CDOM fluorometer) to correct for the covarying production of CDOM. To our knowledge, the production of CDOM by bivalve farms has not been studied.

Other advantages and disadvantages of the method

The main advantages of using moored radiometers to measure diffuse attenuation as a means to assess horizontal gradients of seston depletion are as follows: (1) The measurements are water-column integrated (see Cullen et al. 1997) thus eliminating the effect of a heterogeneous tracer distribution throughout the bivalve stratum. (2) Measurements can be made with a high temporal resolution, thus minimizing problems associated with infrequent sampling such as aliasing (see Taggart and Frank 1990). (3) Measurements of \bar{K} are in absolute units (m^{-1} ; see Cullen et al. 1997); consequently, the output from multiple moorings can be compared without the need of conversion factors or instrument intercalibration that could potentially introduce large errors in the calculated depletion index. (4) These passive optical instruments have low battery requirements, thus they are appropriate for long-term deployments, and (5) the values of \bar{K} are independent of the chlorophyll fluorescence quantum yield; therefore \bar{K} can complement measurements from conventional field fluorometers that may spuriously estimate chlorophyll concentration under high solar irradiance conditions (Falkowski and Kolber 1995; Cullen and Lewis 1995).

Apart from the already mentioned disadvantages of the method regarding the determination of non-tracer attenuating substances, biofouling, frame-shading, wave focusing, resuspension of sediments, and production of biodeposits, other limitations of the method are that (1) measurements cannot be made at night. Therefore, the data are not continuous, hence complicating signal analysis and interpretation, and (2) the cost of the instruments limits the amount of moorings that can be simultaneously deployed, restricting the spatial resolution of the method. Underwater monochromatic radiometers are still approximately three times more expensive than underwater fluorometers (even though radiometers are fundamentally simpler instruments). However, it is expected that underwater radiometers will be produced at more competitive prices as they become more popular.

Discussion

This study demonstrated that the technology and supporting theory is sufficiently developed and ready to use in real-world problems regarding the assessment of horizontal seston gradients produced by bivalve suspension-feeding on regions where there is a naturally occurring tracer that behaves conservatively. However, in sites where the tracer is nonconservative due to strong and continuous sediment resuspension

(from the bottom and/or from the aquaculture ropes), the proposed method cannot be applied without independent measurements to correct for non-tracer particles. Although, we suggested possible solutions to resolve for the resuspended non-tracer particles (i.e., use of transmissometers, optical backscatters, or multi-spectral radiometers), more research is required to demonstrate the efficacy of these suggestions.

This study also demonstrated that \bar{K} from multiple moorings and frequent water samples (analogous to a simple instrument calibration) are enough to assess horizontal gradients of seston caused by bivalve-feeding in environments where non-filterable light attenuating substances (i.e., CDOM) are negligible or remain relatively constant throughout the experiment. For environments where nonfilterable substances are significant and variable, the method is still applicable, but independent measurements are required to correct for the time-varying offset.

The application of this method will be of particular benefit to the field of shellfish aquaculture. Results produced with this method can complement existing seston depletion models (e.g., Bacher et al. 2003; Dowd 2003; Grangeré et al. 2010) applied to the assessment of carrying capacity, which is the major focus of current scientific studies in this field (Bacher et al. 2003; Guyondet et al. 2010; Byron et al. 2011).

In operational aquaculture, the ability to measure bivalve-induced seston gradients will help farmers to make managerial decisions and will help legislative agencies to design and enforce guidelines regarding the usage of the available seston, which may be an issue of growing importance as the available space is occupied and seston supply becomes limiting.

In the field of benthic ecology, the application of the proposed method can result in new insight regarding interactions between natural populations of benthic suspension-feeders and their environment. For example, Huang et al. (2003) assessed tidal and seasonal variations of seston in a saltmarsh inhabited by suspension-feeding ribbed mussels. Seston was assessed approximately every 3 months using column-integrated water samples at hourly intervals for several tide cycles. Huang et al. (2003) showed general patterns in the variability of seston including significant differences between the ebb and flood tides. However, they concluded that seston supply (composition and concentration) was unpredictable and highly variable in time-scales of hours to days. The high temporal resolution measurements of the proposed method could be used in these types of studies to produce years-long time-series that could help in the development of predictive models of seston concentration and quality.

The proposed method can be applied to the study of suspension-feeding invasive bivalves. The method may lead to new insight regarding the invasion ecology of filter-feeders and may be a useful tool to monitor the progress of current invasions. Considering the invasion of the zebra mussel (*Dreissena* spp.) on the Great Lakes as an example, Ackerman et al. (2001) were able to determine significant vertical gradients of

seston, however there was a lack of statistical significance in horizontal gradients. Repeating the experiment using the proposed method could lead to a detailed characterization of the impact of zebra mussel reefs in horizontal scales.

The proposed method can be also used to assess horizontal phytoplankton gradients associated with phenomena other than bivalve filter-feeding, such as sewage discharge or advection of harmful algal blooms. The method can also be applied using other wavelengths to enable measurements of gradients of CDOM or suspended particles associated with other horizontally variable phenomena in the coastal ocean.

Comments and recommendations

Approach design

The most critical aspect to the design of an experiment using the proposed method is to understand the spatial and temporal sources of variation of the different, tracer and non-tracer, light-attenuating substances. These sources of variation will determine the sampling locations, sampling rate, experimental wavelength(s), required ancillary data, etc. In most cases, a trial experiment will be required before the design of the main critical experiment.

Instrument setup

The vertical array of irradiance sensors and the frame should be designed to minimize sensor-shading. If security structures (e.g., radar reflectors) are used, place them poleward from the sensors to minimize shading.

Instrument schedule

Program instruments to measure continuously for approximately 15 s to account for high frequency variability in irradiance associated with wave focusing. During post-collection processing, calculate medians instead of means and measure data at night to assess instrument noise and dark currents (Cullen et al. 1994).

Biofouling considerations

If possible, install shutters and place copper strips around sensors to minimize biofouling (see Manov et al. 2004). In any case, always perform a biofouling assessment (as previously described) before cleaning the sensors.

Alternative means for offset estimation

One particularly critical aspect of the time-varying offset approach is the characterization, using independent data, of the value of non-tracer light-attenuating substances. In this study, we calculated such non-tracer substances using in situ salinity as a proxy for attenuation of CDOM. However, other more direct approaches, such as the use of CDOM fluorometers (WET Labs), in situ spectrophotometers (AC9; WET Labs, Inc.) or multispectral diffuse attenuation meters (multispectral TACCS; Satlantic), can also be used.

Future work

Effort should also be allocated in the assessment of multispectral attenuation, since it may be feasible to use ratios of attenuation coefficients at multiple wavelengths to resolve the concentration of CDOM, tripton, and other attenuating sub-

stances relevant to coastal zone monitoring (see Cullen et al. 1997; Dickey 2003).

It is also important to assess seston aggregation and disaggregation in bivalve farms and the effect that it may cause to the determination of seston depletion using measurements of \bar{K} (i.e., TACCS), beam c attenuation (i.e., transmissometers) and backscattering, which are dependent on the seston size-distribution.

References

- Aas, E., and B. Korsbo. 1997. Self-shading effect by radiance meters on upward radiance observed in coastal waters. *Limnol. Oceanogr.* 42:968-974 [doi:10.4319/lo.1997.42.5.0968].
- Ackerman, J. D., M. R. Loewen, and P. F. Hamblin. 2001. Benthic-pelagic coupling over a zebra mussel reef in western Lake Erie. *Limnol. Oceanogr.* 46:892-904 [doi:10.4319/lo.2001.46.4.0892].
- Bacher, C., J. Grant, A. J. S. Hawkins, J. Fang, M. Zhu, and M. Besnard. 2003. Modelling the effect of food depletion on scallop growth in Sungo Bay (China). *Aquat. Living Resour.* 16:10-24 [doi:10.1016/S0990-7440(03)00003-2].
- Bayne, B. L., J. I. P. Iglesias, A. J. S. Hawkins, E. Navarro, M. Heral, and J. M. Deslous-Paloi. 1993. Feeding behaviour of the mussel, *Mytilus edulis*: responses to variations in quantity and organic content of the seston. *J. Mar. Biol. Assoc. U.K.* 73:813-829 [doi:10.1017/S0025315400034743].
- Berwald, J., D. Stramski, C. D. Mobley, and D. A. Kiefer. 1995. Influences of absorption and scattering on vertical changes in the average cosine of the underwater light field. *Limnol. Oceanogr.* 40:1347:1357 [doi:10.4319/lo.1995.40.8.1347].
- Blough, N. V., O. C. Zafiriou, and J. Bonilla. 1993. Optical absorption spectra of waters from the Orinoco River outflow: Terrestrial input of colored organic matter to the Caribbean. *J. Geophys. Res.* 98:2271-2278 [doi:10.1029/92JC02763].
- Byron, C., J. Link, B. Costa-Pierce, and D. Bengtson. 2011. Calculating ecological carrying capacity of shellfish aquaculture using mass-balance modeling: Narragansett Bay, Rhode Island. *Ecol. Model.* 222(10):1743-1755 [doi:10.1016/j.ecolmodel.2011.03.010].
- Cabanas, J. M., J. J. Gonzalez, J. Mariño, A. Perez, and G. Román. 1979. Estudio del mejillón y de su epifauna en los cultivos flotantes de la Ria de Arosa. III. Observaciones previas sobre la retención de partículas y las biodeposiciones de una batea. *Bol. Inst. Espa. Oceano.* Tomo V. 268:45-50.
- Ciotti, A. M., J. J. Cullen, and M. R. Lewis. 1999. A semi-analytical model of the influence of phytoplankton community on the relationship between light attenuation and ocean color. *J. Geophys. Res.* 104:1559-1578 [doi:10.1029/1998JC900021].
- , M. R. Lewis, and J. J. Cullen. 2002. Assessment of the relationships between dominant cell size in natural phytoplankton communities and the spectral shape of the absorption coefficient. *Limnol. Oceanogr.* 47:404-417

- [doi:10.4319/lo.2002.47.2.0404].
- Cranford, P. J., and B. T. Hargrave. 1994. In situ time-series measurement of ingestion and absorption rates of suspension-feeding bivalves: *Placopecten magellanicus*. *Limnol. Oceanogr.* 39:730-738 [doi:10.4319/lo.1994.39.3.0730].
- Cullen, J. J., A. M. Ciotti, and M. R. Lewis. 1994. Observing biologically induced optical variability in coastal waters. *SPIE Ocean Optics* 2258:105-115.
- , and M. R. Lewis. 1995. Biological processes and optical measurements near the sea surface: some issues relevant to remote sensing. *J. Geophys. Res. C* 100:13255-13266 [doi:10.1029/95JC00454].
- , A. M. Ciotti, R. F. Davis, and M. R. Lewis. 1997. Optical detection and assessment of algal blooms. *Limnol. Oceanogr.* 42:1223-1239 [doi:10.4319/lo.1997.42.5_part_2.1223].
- Dame, R. F., N. Dankers, T. Prins, H. Jongsma, and A. Smaal. 1991. The influence of mussel beds on nutrients in the western Wadden Sea and eastern Scheldt estuaries. *Estuaries* 14:130-138 [doi:10.2307/1351686].
- Dickey, T. D. 2003. Emerging ocean observations for interdisciplinary data assimilation systems. *J. Mar. Syst.* 40:5-48 [doi:10.1016/S0924-7963(03)00011-3].
- Dowd, M. 2003. Seston dynamics in a tidal inlet with shellfish aquaculture: a model study using tracer equations. *Est. Coast. Shelf. Sci.* 57:523-537 [doi:10.1016/S0272-7714(02)00397-9].
- Falkowski, P. G., and Z. Kolber. 1995. Variation in chlorophyll fluorescence yields in phytoplankton in the world oceans. *Aust. J. Plant. Physiol.* 22:341-355 [doi:10.1071/PP9950341].
- Ferreira, J. G., A. J. S. Hawkins, P. Monteiro, and H. Moore. 2008. Integrated assessment of ecosystem-scale carrying capacity in shellfish growing areas. *Aquaculture* 275:138-151 [doi:10.1016/j.aquaculture.2007.12.018].
- Fr chet te, M., and E. Bourget. 1985. Food-limited growth of *Mytilus edulis* L. in relation to the benthic boundary layer. *Can. J. Fish. Aquat. Sci.* 42:1166-1170 [doi:10.1139/f85-144].
- , D. A. Booth, B. Myrand, and H. Berard. 1991. Variability and transport of organic seston near a mussel aquaculture site. *ICES Mar. Sci. Symp.* 192:24-32.
- Granger , K., S. Lefebvre, C. Bacher, P. Cugier, and A. M enesguen. 2010. Modelling the spatial heterogeneity of ecological processes in an intertidal estuarine bay: dynamic interactions between bivalves and phytoplankton. *Mar. Ecol. Prog. Ser.* 415:141-158 [doi:10.3354/meps08659].
- Grant, J., and C. Bacher. 1998. Comparative model of mussel bioenergetics and their validation at field culture sites. *J. Exp. Mar. Bio. Ecol.* 219:21-44 [doi:10.1016/S0022-0981(97)00173-1].
- , C. Bacher, P. J. Cranford, T. Guyondet, and M. Carreau. 2008. A spatially explicit ecosystem model of seston depletion in dense mussel culture. *J. Mar. Syst.* 73:155-168 [doi:10.1016/j.jmarsys.2007.10.007].
- Gregory, D., B. Petrie, F. Jordan, and P. Langille. 1993. Oceanographic, geographic and hydrological parameters of Scotia-Fundy and southern Gulf of St. Lawrence inlets. *Can. Tech. Rep. Hydrog. Ocean. Sci.* 143:viii-248.
- Green, R. E., and H. M. Sosik. 2004. Analysis of apparent optical properties and ocean color models using measurements of seawater constituents in New England continental shelf surface waters. *J. Geophys. Res.* 109:C03026 [doi:10.1029/2003JC001977].
- Guyondet, T., S. Roy, V. G. Koutitonsky, J. Grant, and G. Tita. 2010. Integrating multiple spatial scales in the carrying capacity assessment of a coastal ecosystem for bivalve aquaculture. *J. Sea Res.* 64(3):341-359 [doi:10.1016/j.seares.2010.05.003].
- Heasman, K. G., G. C. Pitcher, C. D. McQuaid, and T. Hecht. 1998. Shellfish mariculture in the benguela system: raft culture of *Mytilus galloprovincialis* and the effect of rope spacing on food extraction, growth rate, production, and condition of mussels. *J. Shellfish Res.* 17:33-39.
- Huang, S. C., D. A. Kreeger, and R. I. E. Newell. 2003. Tidal and seasonal variations in the quantity and composition of seston in a North American, mid-Atlantic saltmarsh. *Est. Coast. Shelf. Sci.* 56:547-560 [doi:10.1016/S0272-7714(02)00205-6].
- Incze, L. S., R. A. Lutz, and E. True. 1981. Modeling carrying capacities for bivalve mollusks in open, suspended-culture systems. *J. World. Aquac. Soc.* 12:143-155.
- Ibarra, D. A. 2003. Estimation of seston depletion by cultured mussels (*Mytilus* spp.) using measurements of diffuse attenuation of solar irradiance from optical moorings. M.Sc. thesis, Dalhousie Univ.
- Johannessen, S. C., and W. L. Miller. 2001. Quantum yield for the photochemical production of dissolved inorganic carbon in seawater. *Mar. Chem.* 76:271-283 [doi:10.1016/S0304-4203(01)00067-6].
- Kirk, J. T. O. 1994. Light and photosynthesis in aquatic ecosystems. Cambridge Univ. Press [doi:10.1017/CBO9780511623370].
- Kotta, J., and F. M ohlenberg. 2002. Grazing impact of *Mytilus edulis* L. and *Dreissena polymorpha* (Pallas) in the Gulf of Riga, Baltic Sea estimated from biodeposition rates of algal pigments. *Ann Zool Fennici* 39:151-160.
- Laanen, M. L., S. W. M. Peters, A. G. Dekker, and H. J. van der Woerd. 2011. Assessment of the scattering by sub-micron particles in inland waters. *J. Eur. Optic. Soc. Rapid Publ.* 6:11046.
- Lee, Z., A. Weidemann, J. Kindle, R. Arnone, K. L. Carder, and C. Davis. 2007. Euphotic zone depth: Its derivation and implication to ocean-color remote sensing. 112:C03009.
- Manov, D. V., G. C. Chang, and T. D. Dickey. 2004. Methods for reducing biofouling of moored optical sensors. *J. Atmos. Ocean. Tech.* 21:958-968 [doi:10.1175/1520-0426(2004)021<0958:MFRBOM>2.0.CO;2].
- Morel, A. 1988. Optical modeling of the upper ocean in rela-

- tion to its biogenous matter content (Case I waters). *J. Geophys. Res.* 93:10749-10768 [doi:10.1029/JC093iC09p10749].
- , and A. Bricaud. 1986. Inherent properties of algal cells including picoplankton: Theoretical and experimental results, p. 521-559. *In* T. Platt and W. K. W. Li [eds.], *Photosynthetic picoplankton*. *Can. Bull. Fish. Aquat. Sci.* 214.
- , and S. Maritorena. 2001. Bio-optical properties of oceanic waters: a reappraisal. *J. Geophys. Res. C. Oceans* 106:7163-7180 [doi:10.1029/2000JC000319].
- Ogilvie, S. C., A. H. Ross, and D. R. Schiel. 2000. Phytoplankton biomass associated with mussel farms in Beatrix Bay, New Zealand. *Aquaculture* 181:71-80 [doi:10.1016/S0044-8486(99)00219-7].
- Piening, B. D., and N. J. McCormick. 2003. Asymptotic optical depths in source free ocean waters. *Appl. Opt.* 42:5382-5387 [doi:10.1364/AO.42.005382].
PMid:14526824
- Pilditch, C. A., J. Grant, and K. R. Bryan. 2001. Seston supply to sea scallops (*Placopecten magellanicus*) in suspended culture. *Can. J. Fish. Aquat. Sci.* 58:241-253 [doi:10.1139/f00-242].
- Piskozov, J. 2004. Effect of 3-D instrument casing shape on the self-shading of in-water upwelling irradiance. *Optics Express*. 12:3144-3148 [doi:10.1364/OPEX.12.003144].
PMid:19483835
- Pope, R. M., and E. S. Fry. 1997. Absorption spectrum (380–700 nm) of pure water. II. Integrating cavity measurements. *Appl. Opt.* 36:8710-8723 [doi:10.1364/AO.36.008710].
PMid:18264420
- Pouvreau, S., C. Bacher, and M. Heral. 2000. Ecophysiological model of growth and reproduction of the black pearl oyster, *Pinctada margaritifera*: potential applications for pearl farming in French Polynesia. *Aquaculture* 2000 186:117-144 [doi:10.1016/S0044-8486(99)00373-7].
- Prins, T. C., A. C. Smaal, A. J. Pouwer, and N. Dankers. 1996. Filtration and resuspension of particulate matter and phytoplankton on an intertidal mussel bed in the Oosterschelde Estuary (SW Netherlands). *Mar. Ecol. Prog. Ser.* 142:121-134 [doi:10.3354/meps142121].
- Rosenberg, R., and L. O. Loo. 1983. Energy-flow in a *Mytilus edulis* culture in Western Sweden. *Aquaculture* 35:151-161 [doi:10.1016/0044-8486(83)90082-0].
- Sathyendranath, S., and T. Platt. 1988. The spectral irradiance field at the surface and in the interior of the ocean: A model for applications in oceanography and remote sensing. *J. Geophys. Res.* 93:9270-9280 [doi:10.1029/JC093iC08p09270].
- Shank, G. C., R. G. Zepp, R. F. Whitehead, and M. A. Moran. 2005. Variations in the spectral properties of freshwater and estuarine CDOM caused by partitioning onto river and estuarine sediments. *Est. Coast. Shelf Sci.* 65:289-301 [doi:10.1016/j.ecss.2005.06.009].
- Smaal, A. C., M. Van Stralen, and E. Schuiling. 2001. The interaction between shellfish culture and ecosystem processes. *Can. J. Fish. Aquat. Sci.* 58:991-1002 [doi:10.1139/f01-026].
- Strickland, J. D. H., and T. R. Parsons. 1972. A practical handbook of seawater analysis. *Bull. Fish. Res. Board. Can.* 167:1-310.
- Strohmeier, T., A. Duinker, Ø. Strand, and J. Aure. 2008. Temporal and spatial variation in food availability and meat ratio in a longline mussel farm (*Mytilus edulis*). *Aquaculture* 276:83-90 [doi:10.1016/j.aquaculture.2008.01.043].
- Sutherland, T. F., C. Leonard, and F. J. R. Taylor. 1992. A segmented pipe sampler for integrated profiling of the upper water column. *J. Plankton Res.* 14:915-923 [doi:10.1093/plankt/14.7.915].
- Taggart, C. T., and K. T. Frank. 1990. Perspectives on larval fish ecology and recruitment processes probing the scales of relationships, p. 151-164. *In* K. Sherman, L. M. Alexander, and B. D. Gold [eds.], *Large marine ecosystems: Patterns, processes, and yields*. American Association for the Advancement of Science.
- Wildish, D., and D. Kristmanson. 1997. *Benthic suspension feeders and flow*. Cambridge Univ. Press [doi:10.1017/CBO9780511529894].
- Zaneveld, J., E. Boss, and A. Bernard. 2001. Influence of surface waves on measured and modeled irradiances profiles. *Appl. Opt.* 40:1442-1449 [doi:10.1364/AO.40.001442].
PMid:18357135
- Zheng, X., T. Dickey, and G. Chang. 2002. Variability of the downwelling diffuse attenuation coefficient with consideration of inelastic scattering. *Appl. Opt.* 42:6477-6488 [doi:10.1364/AO.41.006477].

Submitted 5 March 2012

Revised 25 October 2012

Accepted 2 November 2012